Summer 2004

Numerical simulation of microwave heating of a target with temperature dependent electrical properties in a single-mode cavity

Hoa Kien Tran
New Jersey Institute of Technology

ABSTRACT

NUMERICAL SIMULATION OF MICROWAVE HEATING OF A TARGET WITH TEMPERATURE DEPENDENT ELECTRICAL PROPERTIES IN A SINGLE-MODE CAVITY

by
Hoa Kien Tran

This dissertation extends the work done by Hile and Kriegsmann in 1998 on microwave heating of a ceramic sample in a single-mode waveguide cavity. In that work, they devised a method combining asymptotic and numerical techniques to speed up the computation of electromagnetic fields inside a high-Q cavity in the presence of low-loss target. In our problem, the dependence of the electrical conductivity on temperature increases the complexity of the problem. Because the electrical conductivity depends on temperature, the electromagnetic fields must be recomputed as the temperature varies. We then solve the coupled heat equation and Maxwell's equations to determine the history and distribution of the temperature in the ceramic sample. This complication increases the overall computational effort required by several orders of magnitude.

In their work, Hile and Kriegsmann used the established technique of solving the time-dependent Maxwell's equations with the finite-difference time domain method (FDTD) until a time-harmonic steady state is obtained. Here we replace this technique with a more direct solution of a finite-difference approximation of the Helmholtz equation. The system of equations produced by this finite-difference approximation has a matrix that is large and non-Hermitian. However, we find that it may be splitted into the sum of a real symmetric matrix and a relatively low-rank matrix. The symmetric system represents the discretization of Helmholtz equation inside an empty and truncated waveguide; this system can be solved efficiently with the conjugate gradient method or fast Fourier transform. The low-rank matrix carries the information at the truncated boundaries of the waveguide and the properties of the sample. The rank of this matrix is approximately the sum of twice the number of grid spacings across waveguide and the number of grid points in the target. As a result of the splitting, we can handle this part of the problem by solving a system having as many unknowns as the rank of this matrix.

With the above algorithmic innovations, substantial computational efficiencies have been obtained. We demonstrate the heating of a target having a temperature dependent electrical conductivity. Comparison with computations for constant electrical conductivity demonstrate significant difference in the heating histories. The computational complexity of our approach in comparison with that of using the FDTD solver favors the FDTD method when ultra-fine grids are used. However, in cases where grids are refined simply to reduce asymptotic truncation error, our method can retain its advantages by reducing truncation error through higher-order discretization of the Helmholtz operator.

NUMERICAL SIMULATION OF MICROWAVE HEATING OF A TARGET WITH TEMPERATURE DEPENDENT ELECTRICAL PROPERTIES IN A SINGLE-MODE CAVITY

by
Hoa Kien Tran

A Dissertation
Submitted to the Faculty of
New Jersey Institute of Technology and
Rutgers, The State University of New Jersey – Newark
in Partial Fulfillment of the Requirements for the Degree of
Doctor of Philosophy in Mathematical Sciences

Department of Mathematical Sciences, NJIT
Department of Mathematics and Computer Science, Rutgers-Newark

August 2004

APPROVAL PAGE

NUMERICAL SIMULATION OF MICROWAVE HEATING OF A TARGET WITH TEMPERATURE DEPENDENT ELECTRICAL PROPERTIES IN A SINGLE-MODE CAVITY

Hoa Kien Tran

Dr. Jonathan H. C. Luke, Dissertation Advisor   Date
Professor of Mathematical Sciences, NJIT

Dr. Demetrius T. Papageorgiou, Committee Member   Date
Professor of Mathematical Sciences, NJIT

Dr. Peter G. Petropoulos, Committee Member   Date
Associate Professor of Mathematical Sciences, NJIT

Dr. David C. Stickler, Committee Member   Date
Professor of Mathematical Sciences, NJIT

Dr. Gerald Whitman, Committee Member   Date
Professor of Electrical and Computer Engineering, NJIT

Author: Hoa Kien Tran

Degree: Doctor of Philosophy

Date: August 2004

Undergraduate and Graduate Education:

- Doctor of Philosophy in Mathematical Sciences,
  New Jersey Institute of Technology, Newark, NJ, 2004

- Master of Science in Applied Mathematics,
  New Jersey Institute of Technology, Newark, NJ, 1999

- Bachelor of Science in Applied Mathematics,
  New Jersey Institute of Technology, Newark, NJ, 1998

Major: Mathematical Sciences

Presentations and Publications:

H. Tran and J. Luke, "Transport of Electromagnetic Energy in Models for Dispersive
   Media," *SIAM 50th Anniversary and Annual Meeting*, Society for Industrial and
   Applied Mathematics, Philadelphia, PA, July 8–12, 2002.

To my parents.

ACKNOWLEDGMENT

TABLE OF CONTENTS

TABLE OF CONTENTS
(Continued)

Chapter   **Page**

LIST OF FIGURES

CHAPTER 1

INTRODUCTION

1.1 Volumetric Heating

Heating is a basic industrial operation required for processes ranging from smelting to cooking. Conventionally, heating is achieved by exposing the surface of an object to high temperature. The energy applied to the surface is then transferred inward by thermal conduction. The prime example for this process is an oven with heated atmosphere. Because heating is limited to the surface, this approach is typically slow and nonuniform. In contrast, volumetric heating is a process in which an entire object is heated more or less uniformly throughout its bulk. There are a number of ways to achieve such a task. The simplest example is attaching the object to the terminals of a battery. The battery passes a current through the object, and some energy will dissipate as heat due to the object's electrical resistance. The other methods include electron beams, and radio and microwave radiations. In each method, energy penetrates the object and is deposited directly in its interior which in turn heats up the object. The advantage of using microwave for heating is that it can heat the object rapidly and uniformly.

1.2 Microwave Applicator

The electromagnetic frequency range from 10^8 to 10^{11} Hz is classified as microwave radiation. However, only a few of frequencies (915 MHz, 2.54 GHz, 5.8 GHz and 24.124 GHz) are used in practice to avoid potential interference with applications besides heating. Every heating process requires a delivery system in order to transfer energy to the desired target. In a conventional oven, air is the delivery medium. For microwave heating, the delivery mechanism is a waveguide which allows electromagnetic waves to propagate with little attenuation from the source to the target. In a

1

common configuration, an aperture and a back wall are added to form a cavity housing the target with intention to trap and amplify the waves. For a given frequency, the size of the waveguide dictates the number of propagating modes. In this study, the single mode applicator is chosen in favor of computational simplicity. Microwave applicators using these frequencies can range from few millimeter to hundred of millimeters for a single mode cavity.

Despite its extensive application, microwave heating has its limitations and problems. The most noticeable weakness is cost; its equipment is more expensive than equipment for conventional heating applications. We can heat a conventional oven with any kind of combustible resource while a microwave applicator requires complex systems to generate desired microwave power. The other disadvantage is intrinsic to volumetric heating which is also its advantage. In short, it is heating by electrical resistance. Thus, the process depends mainly on the electrical properties of the object and the intensity of microwave radiation or the input power of the applicator. The input power for a microwave applicator can ranges from a typical home oven of 1 kW to powerful industrial microwave oven of 1 MW or more. Therefore, we can theoretically estimate the dissipated power absorbed by the object for a given microwave applicator. However, the unpredictability of the interaction between microwave and the interior of the object at microscopic level can give rise control difficulties which in the worst possible case can result in thermal runaway and melting the object. In contrast to conventional heating where the oven is heated up to a certain temperature, and the object is heated via thermal convection and radiation. Hence, thermal runaway will never occur in a conventional oven because the object may never be hotter than the surrounding air. In summary, it is more difficult to control the process with microwave heating.

1.3   Ceramic Sample

Ceramics are inorganic materials that are nonmetallic and have crystalline structure. Some of the widely used ceramics include alumina, silicon carbide, and silicon nitride. Ceramics have a wide range of properties that are unique and useful to many applications. For example, silicon nitride is light weight and has excellent thermal shock and wear resistances; as a result, it is used for internal combustion engine parts and gas turbine parts. On the other hand, silicon carbide has high temperature strength and chemical resistance. It is suited for use in applications involving corrosive chemicals such as sulfuric acid.

Since we intend to study the microwave heating process of a ceramic sample, we desire to know their electrical properties. Their electrical properties are widely varied as their physical properties. The electrical conductivities vary on the order of 10^9 for different ceramics. Most are electrical insulators but some have been designed to be superconducting. Their conductivities also can change by several orders of magnitude with temperature variations. The electrical conductivity of some forms of silicon carbide increases by a hundred fold or more as temperature goes from room temperature to 500 °C. The dependence of conductivity on temperature poses a basic challenge for simulating microwave heating of ceramics. To determine the heat deposited in a ceramic, it is necessary to compute the pattern of the electric field. This pattern depends strongly on the conductivity of the material. Hence, the electric field must be recomputed during the heating process. Besides its dependence on temperature, electrical conductivity also depends on frequency. However, most microwave applicators only produce one frequency. Thus, we avoid such consideration in our study by choosing a single frequency applicator.

Typically, ceramics begin as a powder. The powder is then mixed with binders and often water to hold them together for processing or catalyst to speed up the sintering process. Finally, the mixture is shaped into proper form, and is ready for

the sintering process. The sintering process is basically heating the ceramic body to a high temperature below its melting temperature which still allows the sample to retain its shape. As the temperature rises, the surface of ceramic grains soften and fuse with the neighboring grains which reduces the porosity. Furthermore, it is important to heat the sample uniformly to produce uniform structure. Therefore, microwave heating is an attractive method for the sintering process.

1.4   Numerics

Microwave heating involves the interaction of electromagnetic waves with thermal transport in the target body. Hence, it involves coupling Maxwell's equations with heat equation. A fundamental difficulty with this coupling is that in the microwave spectrum the time scale for electromagnetic processes is of the order of a nanosecond while the time scale for heat conduction in a ceramic body of a few centimeters in size is roughly a millisecond. It is well known, however, that this strong contrast in time scales can be used to good advantage in analyzing this problem. The electric field can be treated as a quasi-static time harmonic field satisfying the Helmholtz equation in the problem analyzed here.

Interestingly, in microwave heating applications the numerical solution of the Helmholtz equation is often obtained using finite difference computation of the time-dependent problem until the steady solution emerges [2, 3, 4, 5]. This approach is at best slow when applied in the case of temperature independent electrical properties where the electric field needs to be computed until the transient disturbance is radiated out of the applicator. Hile and Kriegsmann [1] significantly sped up the computational process by inventing a hybrid method. Their method combines FDTD with theory of scattering matrix which separates the iris from the rest of the cavity. Without the iris, there is no resonance; hence, the FDTD converges to the time-harmonic steady state faster than it would in presence of resonant state.

This study further explores their technique for the problem with temperature dependent electrical conductivity using a direct solver for the Helmholtz equation instead of FDTD method. However, direct solver always gives rise to a large system of equations. There had been work done to solve the Helmholtz equation using various methods such as eigenfunction expansion, or multigrid method [6, 7, 8]. For example, Abrahamsson and Kreiss [9] used eigenfunction expansion to solve the Helmholtz equation in a multimode duct where the coupling modes could be reduced to weakly coupled via Riccati transformation. This resulted in partition of the matrix into diagonal dominant blocks which enabled a faster convergence for an iterative scheme. They sped up the method further by splitting into left and right traveling solutions which reduces the boundary value problem into two initial value problems. Their method can be extended to include electromagnetic type problems. However, it requires the traversal eigenfunctions to vary smoothly along the longitudinal direction which may not applicable for our problem because the permittivity and conductivity are discontinuous at the surface of the sample. In [8], Elman and *et al.* showed that their generalized minimal residual (GMRES) multigrid method for the exterior problem converged with fewer iterations than the standard multigrid method. However, it is unclear to us that the method will apply to both the interior and exterior problem such as ours. We note that the discretization of our problem also yields a complex-symmetric matrix as in [8]. However, there is no mention of whether the method could be generalized for any complex-symmetric matrix.

Because of rectangular geometry of the waveguide and the relatively small size of the sample, we split the large matrix into the sum of a real symmetric matrix, which can be solved efficiently using conjugate gradient or fast Fourier transform, and a low-rank matrix. As a result, we reduce to solve a system having as many unknowns as the rank of the low-rank matrix.

CHAPTER 2

DESCRIPTION OF THE PROBLEM

Our objective is to simulate numerically the heating of a ceramic sample in a microwave cavity. The cavity is formed by sectioning the TE_{103} waveguide with a symmetric iris and a movable back wall. The sample is an uniform cross-section cylinder of arbitrary shape which runs from top to bottom of the waveguide as shown in Figure (2.1). Figure (2.2) shows the side view of the cavity. Then, the Maxwell's equations (2.1),
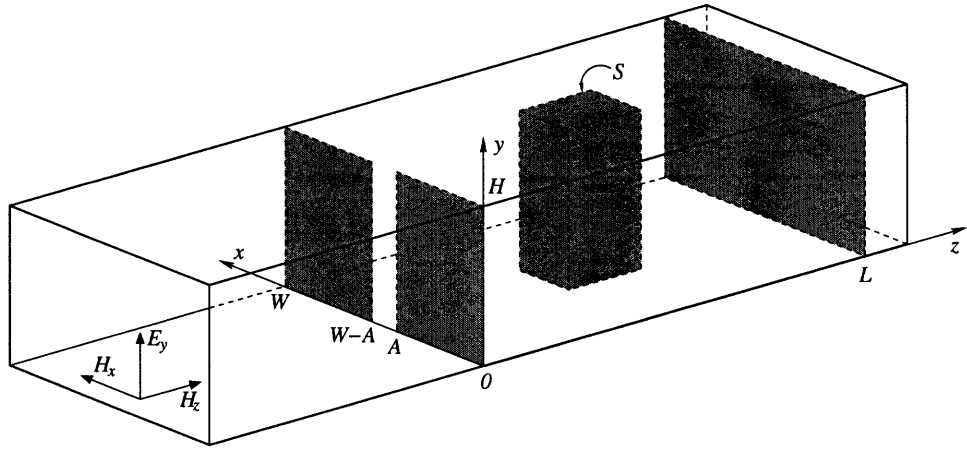
Figure 2.1 Three dimensional view of cavity formation. The cavity has width W, height H and adjustable length L. The aperture of the iris is $W - 2A$.

(prime $'$ denotes dimensional variable)

$$\nabla' \cdot \mathbf{D}' = \varrho', \qquad \nabla' \cdot \mathbf{B}' = 0,$$
$$\nabla' \times \mathbf{E}' = -\frac{\partial \mathbf{B}'}{\partial t'}, \quad \nabla' \times \mathbf{H}' = \frac{\partial \mathbf{D}'}{\partial t'} + \mathbf{J}', \tag{2.1}$$

describe the electric field $\mathbf{E}'$ and magnetic field $\mathbf{H}'$ both inside the cavity and the ceramic sample for appropriate choice of free charge density ϱ' and current density $\mathbf{J}'$. Specifically, there are no free charge and current outside the ceramic sample because the cavity is filled with air; hence, $\varrho' = 0$ and $\mathbf{J}' = \mathbf{0}$. Inside the sample, the
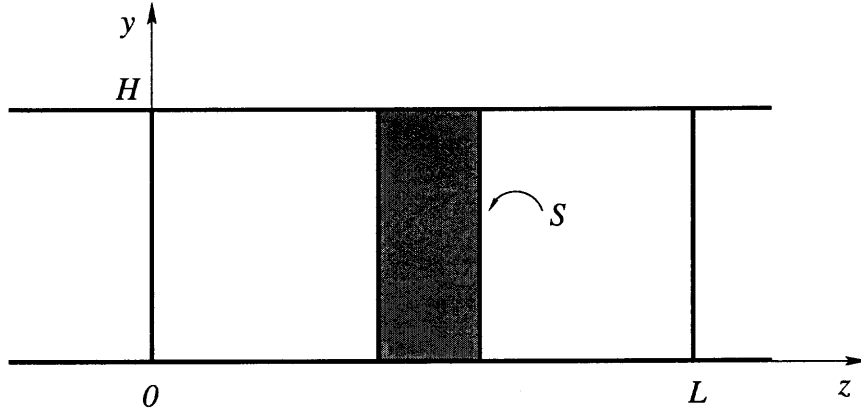
Figure 2.2 The side view of the cavity.

relationship of ϱ' and $\mathbf{J}'$ to the electromagnetic fields are properties of a particular ceramic. Similarly, dielectric displacement $\mathbf{D}'$ and magnetic induction $\mathbf{B}'$ dependence on $\mathbf{E}'$ and $\mathbf{H}'$ also depends on position; e.g. $\mathbf{D}' = \epsilon_0 \mathbf{E}'$ and $\mathbf{B}' = \mu_0 \mathbf{H}'$ for the fields outside the sample. The dielectric displacement and magnetic induction obey a different set of constituent laws inside the sample.

The loaded cavity is then excited by the TE_{10} mode. A portion of the electromagnetic energy is converted to thermal energy by mean of doing work through electrical resistance. This conversion of energy contributes as the heat source for the diffusion equation describing the evolution of temperature of the sample.

$$\rho C_p \frac{\partial T'}{\partial t'} = \nabla' \cdot (\kappa' \nabla' T') + \mathbf{J}' \cdot \mathbf{E}', \tag{2.2}$$

where T' is the temperature of the sample, $\mathbf{J}' \cdot \mathbf{E}'$ is the rate of work done by the field per unit volume, and ρ, C_p and κ' are mass density, heat capacity and thermal conductivity of the sample, respectively.

To close the system, we need to prescribe the boundary conditions at the cavity walls and the sample's surfaces. We are assuming that the cavity walls and iris are perfectly conducting, then the tangential components of electric field vanishes at the

walls, i.e.

$$\mathbf{E}' \times \hat{\mathbf{n}}' = \mathbf{0}. \tag{2.3}$$

At the surface of the sample, we have the continuity of tangential components of electric and magnetic fields.

$$[\mathbf{E}' \times \hat{\mathbf{n}}']_S = \mathbf{0}, \tag{2.4}$$

$$[\mathbf{H}' \times \hat{\mathbf{n}}']_S = \mathbf{0}. \tag{2.5}$$

For the heat equation, we impose a combination of the convective and radiative conditions at the surface of the sample,

$$\kappa' \frac{\partial T'}{\partial n'} = -\eta(T' - T_0) - \mathcal{E}\varsigma(T'^4 - T_0^4), \tag{2.6}$$

where T_0 denotes the ambient temperature, η is natural heat convection coefficient for air, ς is the Stefan-Boltzmann constant which equals to $5.67 \times 10^{-8} \mathrm{Wm}^{-2}\mathrm{K}^{-4}$, and $\mathcal{E}$ is the emissivity of the surface. For an ideal blackbody, the emissivity would be one, and polished surface would have emissivity near zero. The emissivity of all other surfaces ranges between zero and one.

Together with boundary conditions (2.3)–(2.6) at the cavity wall and sample's surface, we can solve the equations (2.1) and (2.2) numerically. However, the difficulty arises when the properties of the sample are temperature dependent; e.g. thermal and electrical conductivities. Since the heat source is generated from electrical resistance, it depends on electrical resistivity or conductivity of the material. Like most physical properties, electrical conductivity varies with temperature which makes the numerical computation rather expensive. For each time step in the numerical method for heat equation, we have to recompute the effective electrical conductivity. The electrical conductivity in turn change the current density $\mathbf{J}'$ which requires updating the electro-

magnetic fields. The updated fields are then fed back into the heat equation as the source. The same process repeats at the next time step.

Depending on the geometry and properties of the sample together with the position of the back wall, the fields inside the cavity can become resonant, which in turn can rapidly heat the sample. Since the fields change with temperature variation, the resonant length varies with temperature. Hence, by adjusting the position of the back wall, we can control the field strength inside the cavity as well as the heating process. It also possible that the sample may not heat appreciably with certain geometry or properties. For example, a slab with high conductivity would act like a back wall of the cavity.

CHAPTER 3

ANALYSIS OF PDE'S

We assume the sample is an isotropic and non-magnetic material with no free charge, i.e.

$$\varrho' = 0, \ \mathbf{D}' = \epsilon'\mathbf{E}', \ \text{and} \ \mathbf{B}' = \mu_0\mathbf{H}'.$$

Then, $\nabla' \cdot (\epsilon'\mathbf{E}') = \nabla'\epsilon' \cdot \mathbf{E}' + \epsilon'\nabla' \cdot \mathbf{E}' = 0$. Although permittivity ϵ' is discontinuous across the sample's surface, the electric field $\mathbf{E}'$ is parallel to the surface. Therefore, $\nabla'\epsilon' \cdot \mathbf{E}'$ term vanishes, and the Maxwell's equations reduce to,

$$
\begin{aligned}
\nabla' \cdot \mathbf{E}' &= 0, & \nabla' \cdot \mathbf{H}' &= 0, \\
\nabla' \times \mathbf{E}' &= -\mu_0\frac{\partial \mathbf{H}'}{\partial t'}, & \nabla' \times \mathbf{H}' &= \epsilon'\frac{\partial \mathbf{E}'}{\partial t'} + \sigma'\mathbf{E}',
\end{aligned}
\tag{3.1}
$$

where we have assumed $\mathbf{J}' = \sigma'\mathbf{E}'$ which is Ohm's law for electrical resistance. We note that ϵ' and σ' are generally frequency dependent in complex media; this dependence plays a significant role in our considerations as we study single frequency applications. The temperature in the target is governed by the heat equation with new source term.

$$\rho C_p\frac{\partial T'}{\partial t'} = \nabla' \cdot (\kappa'\nabla'T') + \sigma'(T')\left|\mathbf{E}'\right|^2. \tag{3.2}$$

In general, the effective conductivity of the sample σ' depends on temperature. Because of such dependence, the Maxwell's equations are coupled with the heat equation. However, it is possible to minimize the computational impact of this coupling by exploiting the different time scales of the problem. We note that κ' also is often strongly temperature dependent over the temperature ranges typical in ceramic processing. However, we do not explore this aspect of the problem in this work.

3.1 Time Harmonic Equations

In microwave heating the microwave source, typically a magnetron, is time harmonic. Therefore, we expect the response of the fields is also time harmonic, i.e. the fields have time dependence $e^{-i\omega t'}$. However, the fields are physical quantities, we choose the real part of the complex solution.

$$\mathbf{E}'(\mathbf{x}', t') = \frac{1}{2}\left[\hat{\mathbf{E}}(\mathbf{x}')e^{-i\omega t'} + \hat{\mathbf{E}}^*(\mathbf{x}')e^{i\omega t'}\right],$$

$$\mathbf{H}'(\mathbf{x}', t') = \frac{1}{2}\left[\hat{\mathbf{H}}(\mathbf{x}')e^{-i\omega t'} + \hat{\mathbf{H}}^*(\mathbf{x}')e^{i\omega t'}\right].$$

Plugging these into equations (3.1), we obtain the time harmonic Maxwell's equations.

$$\nabla' \cdot \hat{\mathbf{E}} = 0, \qquad \nabla' \cdot \hat{\mathbf{H}} = 0,$$

$$\nabla' \times \hat{\mathbf{E}} = i\mu_0\omega\hat{\mathbf{H}}, \quad \nabla' \times \hat{\mathbf{H}} = -i\epsilon'\omega\hat{\mathbf{E}} + \sigma'\hat{\mathbf{E}}.$$

While the heat source $\sigma' |\mathbf{E}'|^2$ is expanded as,

$$\sigma' |\mathbf{E}'|^2 = \frac{\sigma'}{2}|\hat{\mathbf{E}}|^2 + \frac{\sigma'}{2}\left(\hat{\mathbf{E}} \cdot \hat{\mathbf{E}}e^{-2i\omega t'} + \hat{\mathbf{E}}^* \cdot \hat{\mathbf{E}}^*e^{2i\omega t'}\right) \tag{3.3}$$

Evidently, there are at least two time scales to the problem. The oscillation time of the electromagnetic fields which is represented by the reciprocal of angular frequency ω. The diffusion time is the ratio of thermal diffusivity $\dfrac{\kappa'}{\rho C_p}$ to area. For microwave application, the oscillation time is on the order of nanosecond. On the other hand, the thermal diffusivity for a very good thermal conductor such as silver is about 170 squared millimeters per second at room temperature. Hence, for the sample of centimeter size, the diffusion time is on the order of milliseconds which is significantly slower than the oscillation time.

3.2 Time Average Equations

For the difference of time scales on order of million, it is conventional to use time average in the equation of slower time. Thus, the time average of the heat equation

over one cycle of oscillation is,

$$\frac{\omega}{2\pi} \int_{t'}^{t' + \frac{2\pi}{\omega}} \rho C_p \frac{\partial T'}{\partial s} \, ds = \frac{\omega}{2\pi} \int_{t'}^{t' + \frac{2\pi}{\omega}} \nabla' \cdot (\kappa' \nabla' T') \, ds + \frac{\omega}{2\pi} \int_{t'}^{t' + \frac{2\pi}{\omega}} \sigma' \, |\mathbf{E}'|^2 \, ds. \quad (3.4)$$

Defining time-average temperature over one period as,

$$\hat{T}(\mathbf{x}', t') = \frac{\omega}{2\pi} \int_{t'}^{t' + \frac{2\pi}{\omega}} T'(\mathbf{x}', s) \, ds.$$

Then, according to fundamental theorem of calculus,

$$\frac{\partial}{\partial t'} \hat{T}(\mathbf{x}', t') = \frac{\omega}{2\pi} \left[T'\left(\mathbf{x}', t' + \frac{2\pi}{\omega}\right) - T'(\mathbf{x}', t') \right].$$

This implies that we can interchange integration and differentiation in equation (3.4). In absence of thermal runaway, we assume that temperature variation is small over a period of oscillation based on the existence of time scales difference. Hence,

$$T'\left(\mathbf{x}', t' + \frac{2\pi}{\omega}\right) \approx T'(\mathbf{x}', t') + \frac{2\pi}{\omega} \frac{\partial T'}{\partial t'},$$

and

$$\hat{T}(\mathbf{x}', t') \approx T'(\mathbf{x}', t') + \frac{\pi}{\omega} \frac{\partial T'}{\partial t'}.$$

Using above approximations to simplify the diffusion and source terms in equation (3.4), i.e.

$$\kappa'\left(T'\left(\mathbf{x}', s\right)\right) \approx \kappa'\left(T'(\mathbf{x}', t') + (s - t')\frac{\partial T'}{\partial t'}\right) \approx \kappa'(\hat{T}(\mathbf{x}', t')) + \left(s - t' - \frac{\pi}{\omega}\right) \frac{\partial \kappa'}{\partial \hat{T}} \frac{\partial T'}{\partial t'}.$$

The diffusion term becomes,

$$\frac{\omega}{2\pi} \nabla \cdot \int_{t'}^{t' + \frac{2\pi}{\omega}} \left[\kappa'(\hat{T}(\mathbf{x}', t')) + \left(s - t' - \frac{\pi}{\omega}\right) \frac{\partial \kappa'}{\partial \hat{T}} \frac{\partial T'}{\partial t'} \right] \nabla' T' \, ds$$

$$= \nabla' \cdot [\kappa'(\hat{T}) \nabla' \hat{T}] + O\left(\frac{\pi}{\omega}\right).$$

The approximation is valid as long as $\frac{\partial \kappa'}{\partial \hat{T}} \ll \frac{1}{\omega}$. Such violation occurs in event of thermal runaway. Similarly, the effective electric conductivity can be approximated,

$$\sigma'\left(T'\left(\mathbf{x}', s\right)\right) \approx \sigma'(\hat{T}(\mathbf{x}', t')) + \left(s - t' - \frac{\pi}{\omega}\right) \frac{\partial \sigma'}{\partial \hat{T}} \frac{\partial T'}{\partial t'},$$

provided $\frac{\partial \sigma'}{\partial \hat{T}} \ll \frac{1}{\omega}$. Using equation (3.3), the source term is simplified to,

$$\frac{\sigma'(\hat{T})}{2}|\hat{\mathbf{E}}|^2 + \frac{\sigma'(\hat{T})}{2}\left[\hat{\mathbf{E}} \cdot \hat{\mathbf{E}} \frac{\omega}{2\pi} \int_{t'}^{t'+\frac{2\pi}{\omega}} e^{-2i\omega s}\, ds + \hat{\mathbf{E}}^* \cdot \hat{\mathbf{E}}^* \frac{\omega}{2\pi} \int_{t'}^{t'+\frac{2\pi}{\omega}} e^{2i\omega s}\, ds\right].$$

Since integration of a periodic function over its period is zero, the time average heat equation becomes,

$$\rho C_p \frac{\partial \hat{T}}{\partial t'} = \nabla' \cdot [\kappa'(\hat{T})\nabla'\hat{T}] + \frac{\sigma'}{2}(\hat{T})|\hat{\mathbf{E}}|^2. \tag{3.5}$$

3.3   Non-Dimensionalization

We re-scale the variables as follow:

$$\mathbf{E} = \frac{\hat{\mathbf{E}}}{E_0}, \quad \mathbf{H} = \sqrt{\frac{\mu_0}{\epsilon_0}} \frac{\hat{\mathbf{H}}}{E_0}, \quad \mathbf{x} = \frac{\mathbf{x}'}{W}, \quad t = \frac{\kappa_0 t'}{\rho C_p W^2}, \text{ and } T = \frac{\hat{T}}{T_0},$$

where W is the waveguide's width, T_0 is the ambient temperature and $\kappa_0 = \kappa'(T_0)$. The dimensionless Maxwell's equations are,

$$\begin{aligned}
\nabla \cdot \mathbf{E} = 0, & \qquad \nabla \cdot \mathbf{H} = 0, \\
\nabla \times \mathbf{E} = -ik\mathbf{H}, & \quad \nabla \times \mathbf{H} = ik\epsilon\mathbf{E} + k\sigma(T)\mathbf{E},
\end{aligned} \tag{3.6}$$

where dimensionless wavenumber $k = \frac{\omega W}{c}$ with c as speed of light, dielectric constant $\epsilon = \frac{\epsilon'}{\epsilon_0}$, and dimensionless conductivity $\sigma(T) = \frac{\sigma'(\hat{T})}{\epsilon_0 \omega}$. And, the dimensionless heat equation is,

$$\frac{\partial T}{\partial t} = \nabla \cdot [\kappa(T)\nabla T] + \sigma(T)\frac{t_{\text{diff}}}{t_{\text{oscill}}}\frac{\frac{\epsilon_0}{2}E_0^2}{\rho C_p T_0}|\hat{\mathbf{E}}|^2,$$

where $\kappa(T) = \dfrac{\kappa'(\hat{T})}{\kappa_0}$, diffusion time $t_{\text{diff}} = \dfrac{\rho C_p W^2}{\kappa_0}$ and oscillation time $t_{\text{oscill}} = \dfrac{1}{\omega}$.

Due to the choice of numerical method, we eliminate the magnetic field $\mathbf{H}$ from equation (3.6) which will give us the Helmholtz equation.

$$\nabla^2 \mathbf{E} + k^2[\epsilon + i\sigma(T)]\mathbf{E} = 0. \qquad (3.7)$$

By the choice of simple geometry for the ceramic sample, e.g. a post with uniform cross-section, we limit the problem to two dimensional. Together with the use of single mode TE cavity, only y-component of the electric field is nonzero. Thus, the equation (3.7) to a scalar equation for E_y.

$$\nabla^2 E_y + k^2[\epsilon + i\sigma(T)]E_y = 0. \qquad (3.8)$$

The boundary condition (2.3) guarantees that E_y vanishes at the cavity's walls while the equation (2.4) implies the continuity of E_y across the surface of the sample. The continuity of magnetic field (2.5) requires some algebraic manipulation to express in term of E_y. From equation (3.6),

$$\mathbf{H} = \frac{i}{k}\nabla \times \mathbf{E} = \frac{i}{k}\left(-\frac{\partial E_y}{\partial z}\hat{\mathbf{x}} + \frac{\partial E_y}{\partial x}\hat{\mathbf{z}}\right).$$

Since we reduce the problem to two dimensional, the unit normal vector of the sample's surface also lies on the two dimensional plane; i.e. $\hat{\mathbf{n}} = n_x\hat{\mathbf{x}} + n_z\hat{\mathbf{z}}$. Thus,

$$[\mathbf{H} \times \hat{\mathbf{n}}]_S = \left[\frac{\partial E_y}{\partial n}\hat{\mathbf{y}}\right]_S = 0,$$

which is the continuity of normal derivative of E_y across the surface of the sample.

3.4 Partition of the Problem

Due to the geometry of the sample, the electric field inside the cavity remains parallel to the y-axis provided the incident electric field points in y direction. Then, we know

the general solution of Helmholtz equation inside the cavity and outside the sample via separation of variables. The modal representation of the solution is,

$$E_y = \sum_{m=1}^{\infty} \left(E_m^r e^{ik_m z} + E_m^\ell e^{-ik_m z} \right) \sin \left(m\pi x \right),$$

where dimensionless wavenumber $k_m = \sqrt{k^2 - m^2 \pi^2}$. As m increases, k_m decreases and eventually becomes purely imaginary for $m > M$. This means that there are M propagating modes and the rest are evanescent modes which decay exponentially along z. We then separate the solution into two parts, the propagating sum and sum that decayed to zero.

$$\begin{aligned} E_y &= \sum_{m=1}^{M} \left(E_m^r e^{ik_m z} + E_m^\ell e^{-ik_m z} \right) \sin \left(m\pi x \right) \\ &+ \sum_{m=M+1}^{\infty} \left(E_m^r e^{ik_m z} + E_m^\ell e^{-ik_m z} \right) \sin \left(m\pi x \right) \end{aligned}$$

Suppose the loaded cavity is excited by the jth propagating mode, the incident mode is diffracted by the iris and creates a full spectrum of modes as a result. Part of it will enter the cavity and is further diffracted by the sample. From the modal expansion and definition of dimensionless wavenumber k_m, we know that $(M+1)^{\text{th}}$ mode is the dominate evanescent mode because it decays slowest in comparison to other evanescent modes. So, at some distance away from the aperture and the sample, the magnitude of the wave corresponds to the $(M+1)^{\text{th}}$ mode will become insignificantly small compared to the magnitude of propagating modes. Because of such decay characteristics of waveguide, we intend to divide the problem into multiple subproblems in hoping to achieve a smaller computation domain [1]. Specifically, the objective is to determine the electric field inside the cavity, but it is impractical to add an infinite number of terms even if we manage to obtain the coefficients. Alternatively, we compute the field numerically. However, the evanescent modes decay away from disturbance. Since we can add a finite number of propagating modes, it is logically

to reduce the computation domain to a smaller region where evanescent modes are insignificant. As shown in Figure (3.1), let z_l and z_r be two imaginary planes where
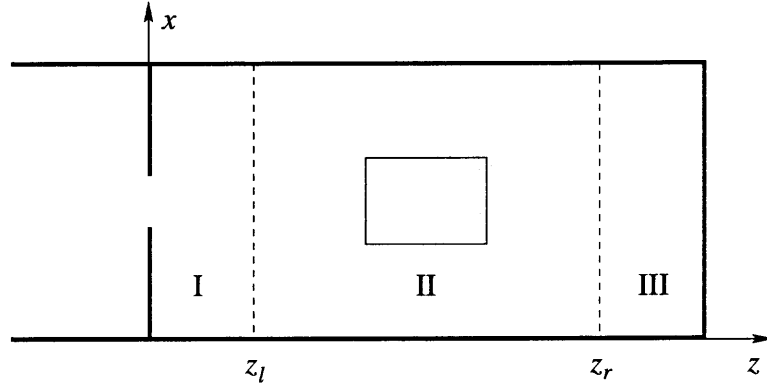
Figure 3.1 Partition of the cavity into multiple regions.

all the evanescent modes diffracted from the aperture and sample are small. Then, splicing the domain at z_l and z_r will divide the problem into three regions I, II, and III. The region III has the simplest problem; a wave composed of M propagating modes impinge on a perfectly conducting wall. Therefore, it is simply reflect back with a determinable phase shift. Regions I and II become the problems of determining the field in a infinite waveguide with an obstacle. Three subproblems can be rejoined using scattering matrices, and the scattering matrix for the region I can be obtained asymptotically. We effectively reduce the computation domain to a smaller area of region II.

Considering a object centered at the $z = 0$ in an infinite waveguide. Let F_m^ℓ and F_m^r be the left and right incident modes, respectively. The electric field away from $z = 0$ is determined asymptotically as,

$$E_y(x, z) = \begin{cases} \displaystyle\sum_{m=1}^{M} \left(F_m^\ell e^{ik_m z} + G_m^\ell e^{-ik_m z} \right) \sin(m\pi x), & z \ll 0, \\ \displaystyle\sum_{m=1}^{M} \left(F_m^r e^{-ik_m z} + G_m^r e^{ik_m z} \right) \sin(m\pi x), & z \gg 0. \end{cases}$$

G_m^ℓ and G_m^r are identified as the linear combinations of reflected and transmitted coefficients corresponding to the modes of incident waves. They relate to the incident modes via a scattering matrix.

$$
\begin{pmatrix} G_1^\ell \\ G_2^\ell \\ \vdots \\ G_M^\ell \\ G_1^r \\ G_2^r \\ \vdots \\ G_M^r \end{pmatrix} = \begin{pmatrix} R_1^1 & R_1^2 & \cdots & R_1^M & T_1^1 & T_1^2 & \cdots & T_1^M \\ R_2^1 & R_2^2 & \cdots & R_2^M & T_2^1 & T_2^2 & \cdots & T_2^M \\ \vdots & \vdots & \ddots & \vdots & \vdots & \vdots & \ddots & \vdots \\ R_M^1 & R_M^2 & \cdots & R_M^M & T_M^1 & T_M^2 & \cdots & T_M^M \\ T_1^1 & T_1^2 & \cdots & T_1^M & R_1^1 & R_1^2 & \cdots & R_1^M \\ T_2^1 & T_2^2 & \cdots & T_2^M & R_2^1 & R_2^2 & \cdots & R_2^M \\ \vdots & \vdots & \ddots & \vdots & \vdots & \vdots & \ddots & \vdots \\ T_M^1 & T_M^2 & \cdots & T_M^M & R_M^1 & R_M^2 & \cdots & R_M^M \end{pmatrix} \begin{pmatrix} F_1^\ell \\ F_2^\ell \\ \vdots \\ F_M^\ell \\ F_1^r \\ F_2^r \\ \vdots \\ F_M^r \end{pmatrix}, \tag{3.9}
$$

where R_m^j and T_m^j are the reflection and transmission coefficients of mth mode excited by the jth mode. Thus, the asymptotic solution away from the iris and the sample excited by the jth mode of unit strength is,

$$
E_y = \begin{cases} e_j^{\text{T}}\phi(x,z) + \rho_i^{\text{T}}\phi^*(x,z), & z \ll z_i, \\ \tau_i^{\text{T}}\phi(x,z) + \rho_t^{\text{T}}\phi^*(x,z), & z_i \ll z \ll z_t, \\ \tau_t^{\text{T}}\phi(x,z) + \rho_w^{\text{T}}\phi^*(x,z), & z_t \ll z, \end{cases} \tag{3.10}
$$

where $\phi(x,z) = (e^{ik_1 z}\sin(\pi x), e^{ik_2 z}\sin(2\pi x), \ldots, e^{ik_M z}\sin(M\pi x))^{\text{T}}$, e_j is the jth standard basis, and ρ_i, τ_i, ρ_t, τ_t, ρ_w are column vectors as shown in Figure (3.2). Rewriting the first two expressions of equation (3.10) by shifting the location of the iris z_i to the origin.

$$
E_y = \begin{cases} e_j^{\text{T}}D_i\phi(x,z-z_i) + \rho_i^{\text{T}}D_i^{\text{H}}\phi^*(x,z-z_i), & z \ll z_i, \\ \tau_i^{\text{T}}D_i\phi(x,z-z_i) + \rho_t^{\text{T}}D_i^{\text{H}}\phi^*(x,z-z_i), & z_i \ll z \ll z_t, \end{cases}
$$
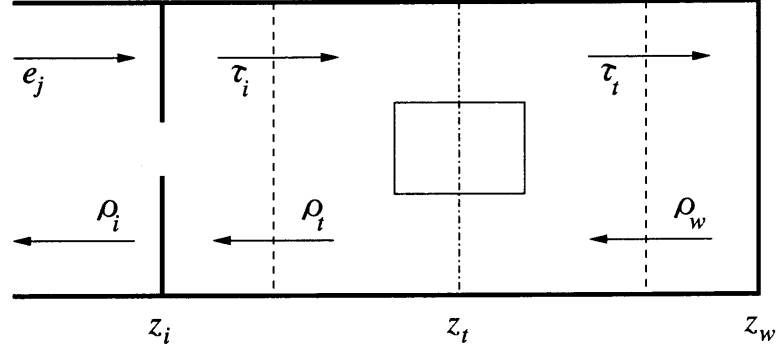
Figure 3.2 Asymptotic solutions.

where $D_i = \text{diag}\left(e^{ik_m z_i}\right)$. Let R_i and T_i be M-by-M block matrices as in equation (3.9) representing the reflection and transmission about the aperture. Then,

$$
\begin{pmatrix} D_i^{\mathrm{H}} \rho_i \\ D_i \tau_i \end{pmatrix} = \begin{pmatrix} R_i & T_i \\ T_i & R_i \end{pmatrix} \begin{pmatrix} D_i e_j \\ D_i^{\mathrm{H}} \rho_t \end{pmatrix}
$$

Since D_i^{H} is the inverse of D_i, above system reduces to,

$$
\begin{pmatrix} \rho_i \\ \tau_i \end{pmatrix} = \begin{pmatrix} D_i R_i D_i & D_i T_i D_i^{\mathrm{H}} \\ D_i^{\mathrm{H}} T_i D_i & D_i^{\mathrm{H}} R_i D_i^{\mathrm{H}} \end{pmatrix} \begin{pmatrix} e_j \\ \rho_t \end{pmatrix}
\tag{3.11}
$$

Similarly, the coefficients about the sample satisfy the following system.

$$
\begin{pmatrix} D_t^{\mathrm{H}} \rho_t \\ D_t \tau_t \end{pmatrix} = \begin{pmatrix} R_\ell & T_r \\ T_\ell & R_r \end{pmatrix} \begin{pmatrix} D_t \tau_i \\ D_t^{\mathrm{H}} \rho_w \end{pmatrix}
$$

where R_ℓ and T_ℓ are reflection and transmission matrices corresponding to an incident wave from the left of the sample while R_r and T_r are reflection and transmission matrices from the right incident wave. In general, R_ℓ is not equal to R_r, and T_ℓ is not equal to T_r because of temperature dependent of electrical conductivity or asymmetrical geometry of the sample. D_t has the same structure as D_i with the center of the sample, z_t, replaces z_i. Hence, ρ_t and τ_t can be expressed in term of

incident waves τ_i and ρ_w as,

$$\begin{pmatrix} \rho_t \\ \tau_t \end{pmatrix} = \begin{pmatrix} D_t R_\ell D_t & D_t T_r D_t^{\mathrm{H}} \\ D_t^{\mathrm{H}} T_\ell D_t & D_t^{\mathrm{H}} R_r D_t^{\mathrm{H}} \end{pmatrix} \begin{pmatrix} \tau_i \\ \rho_w \end{pmatrix} \tag{3.12}$$

At the short $z = z_w$, the field is zero. Hence, the last expression of Eq. (3.10),

$$D_w \tau_t + D_w^{\mathrm{H}} \rho_w = 0 \tag{3.13}$$

Combining Eq. (3.11), Eq. (3.12) and Eq. (3.13),

$$\begin{pmatrix} I & 0 & -D_i T_i D_i^{\mathrm{H}} & 0 & 0 \\ 0 & I & -D_i^{\mathrm{H}} R_i D_i^{\mathrm{H}} & 0 & 0 \\ 0 & -D_t R_\ell D_t & I & 0 & -D_t T_r D_t^{\mathrm{H}} \\ 0 & -D_t^{\mathrm{H}} T_\ell D_t & 0 & I & -D_t^{\mathrm{H}} R_r D_t^{\mathrm{H}} \\ 0 & 0 & 0 & D_w & D_w^{\mathrm{H}} \end{pmatrix} \begin{pmatrix} \rho_i \\ \tau_i \\ \rho_t \\ \tau_t \\ \rho_w \end{pmatrix} = \begin{pmatrix} D_i R_i D_i e_j \\ D_i^{\mathrm{H}} T_i D_i e_j \\ 0 \\ 0 \\ 0 \end{pmatrix} \tag{3.14}$$

Although we limited ourselves to single mode cavity, the above analysis would serve well in the situation where we want to reduce the computational domain around the sample. In such situation, some evanescent modes that decay slowly would not be negligible at the truncated boundaries; hence, they would be included into the computation.

3.5   Resonant Length

For a single mode waveguide, the system (3.14) reduces to,

$$\begin{pmatrix} 1 & 0 & -T_i & 0 & 0 \\ 0 & 1 & -R_i^- & 0 & 0 \\ 0 & -R_\ell^+ & 1 & 0 & -T_r \\ 0 & -T_\ell & 0 & 1 & -R_r^- \\ 0 & 0 & 0 & e^{ik_1 z_w} & e^{-ik_1 z_w} \end{pmatrix} \begin{pmatrix} \rho_i \\ \tau_i \\ \rho_t \\ \tau_t \\ \rho_w \end{pmatrix} = \begin{pmatrix} R_i^+ \\ T_i \\ 0 \\ 0 \\ 0 \end{pmatrix} \tag{3.15}$$

where $R_i^+ = R_i e^{2ik_1 z_i}$, $R_i^- = R_i e^{-2ik_1 z_i}$, $R_\ell^+ = R_\ell e^{2ik_1 z_t}$ and $R_r^- = R_r e^{-2ik_1 z_t}$. We can solve for ρ_i, τ_i, ρ_t, τ_t and ρ_w given the R's and T's. R_i and T_i are the reflection and transmission coefficients of the iris are computed asymptotically; the analysis of the asymptotic method is shown in §A.1. The first two terms in the asymptotic series for R_i and T_i are,

$$R_i = \frac{-ib}{1+ib}, \text{ and } T_i = 1 + R_i,$$
$$\text{where } b = \frac{\pi}{k_1}\left[\tan^2(\pi a) - \frac{3\delta_3 \sin^4(\pi a)}{1 - \delta_3 \cos^6(\pi a)}\right],$$
$$\text{and } \delta_3 = 1 - \sqrt{1 - \frac{k^2}{9\pi^2}}.$$

While R_ℓ, R_r, T_ℓ and T_r are obtained numerically by solving the infinite waveguide in presence of an obstacle problem.

To optimize the heating process, we look at the coefficient ρ_i. We know that ρ_i is the coefficient of the reflected wave from the cavity. For a cavity loaded with a lossless sample, we expect the magnitude of ρ_i to be unity. For a lossy sample, the magnitude of ρ_i is less than unity because some electromagnetic energy is absorbed by the sample. Therefore, we are interested in the cavity length for which the sample absorbs the most electromagnetic energy. Since $1 - |\rho_i|^2$ represents the loss of energy due to absorption, we can find the optimal length by maximize the energy loss or minimize the reflected energy, i.e. $|\rho_i|^2$. By Crammer's rule, we obtain

$$\rho_i = \frac{\left[R_i^+ R_r^- - (R_i^2 - T_i^2)(R_\ell R_r - T_\ell T_r)\right] e^{2ik_1 z_w} + R_i^+ - (R_i^2 - T_i^2) R_\ell^+}{\left[R_r^- - R_i^-(R_\ell R_r - T_\ell T_r)\right] e^{2ik_1 z_w} + 1 - R_i^- R_\ell^+}.$$

We recognize that ρ_i is a linear fraction transformation that maps a unit circle $e^{2ik_1 z_w}$ centered at origin to another circle in ζ-plane. Let Γ be the image of the unit circle $e^{2ik_1 z_w}$ via the transformation, then minimizing $|\rho_i|^2$ is the same as finding a point on the circle Γ closest to the origin. And this point is the intersection of the circle Γ
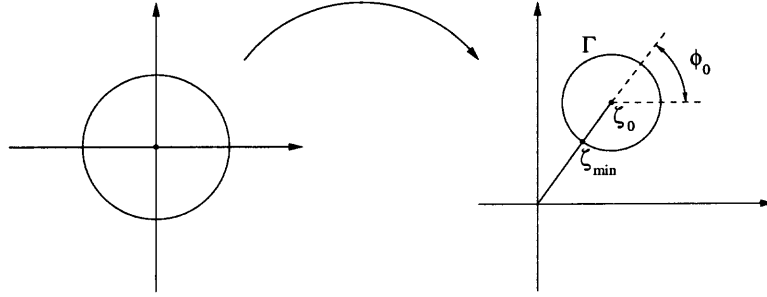
Figure 3.3 Finding the minimum via linear fraction transformation.

with the segment connected its center and origin as show in Figure (3.3).

$$\zeta_{\min} = \zeta_0 - \varrho e^{i\phi_0}$$

where circle Γ is defined as $\zeta_0 + \varrho e^{i\phi}$, and ϕ_0 is the argument of ζ_0. Hence,

$$e^{2ik_1 z_w} = \frac{\left(1 - R_i^- R_\ell^+\right) \zeta_{\min} - \left[R_i^+ - (R_i^2 - T_i^2) R_\ell^+\right]}{-\left[R_r^- - R_i^- (R_\ell R_r - T_\ell T_r)\right] \zeta_{\min} + \left[R_i^+ R_r^- - (R_i^2 - T_i^2)(R_\ell R_r - T_\ell T_r)\right]}.$$

Figures (3.4) and (3.5) show the fields inside a cavity of width 109.2 mm for various locations of the back wall. The cavity is loaded with a square post of size 40.1 mm centered at $x = 54.6$ mm and $z = 144.9$ mm. The effective electrical conductivity of the post is 5×10^{-4} $\Omega^{-1} \text{m}^{-1}$, and its dielectric constant is 9.7. The most noticeable difference of Figures (3.4) and (3.5) is the huge gap in the magnitude of the electric field. Figure (3.4) plots the magnitude of the dimensionless electric field when the cavity set to the optimal length, the the maximum strength inside the sample is about 27. Whereas, the electric field in Figure (3.5) occurs when the position of the back wall corresponding to the least amount energy deposited into the sample. Therefore, the electric field inside the sample is very small; its maximum is 0.06. Figure (3.4) also show some interesting behavior of electric field; i.e. the electric field inside a lossy sample is larger than its surrounding. It is simply a coincidence that we place the sample at optimal location. If we move the sample about 17 mm along cavity, we
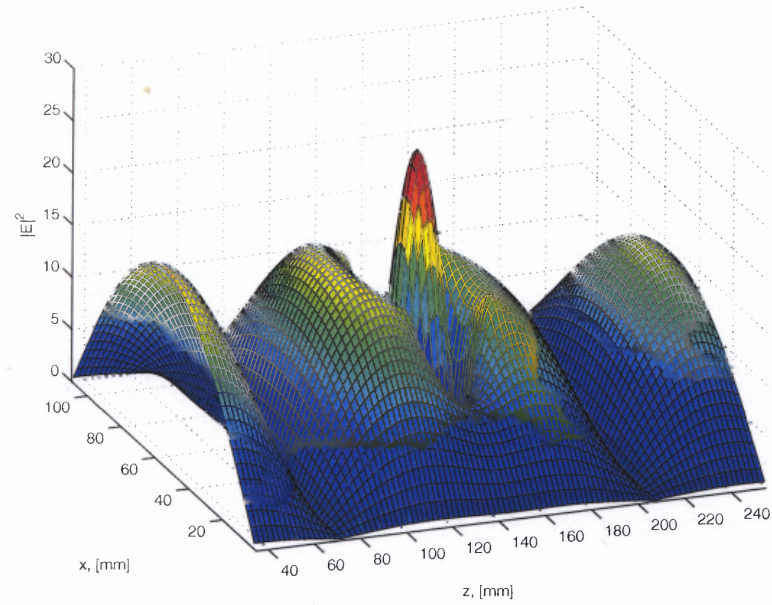
Figure 3.4 Magnitude of electric field inside a cavity when $|\rho_i|^2$ is at its minimum. The center of post locates at $x = 54.6$ mm and $z = 144.9$ mm.

observe entirely differently behavior as shown in Figure (3.6). This demonstrates that the heating process also depends on where we place the sample.
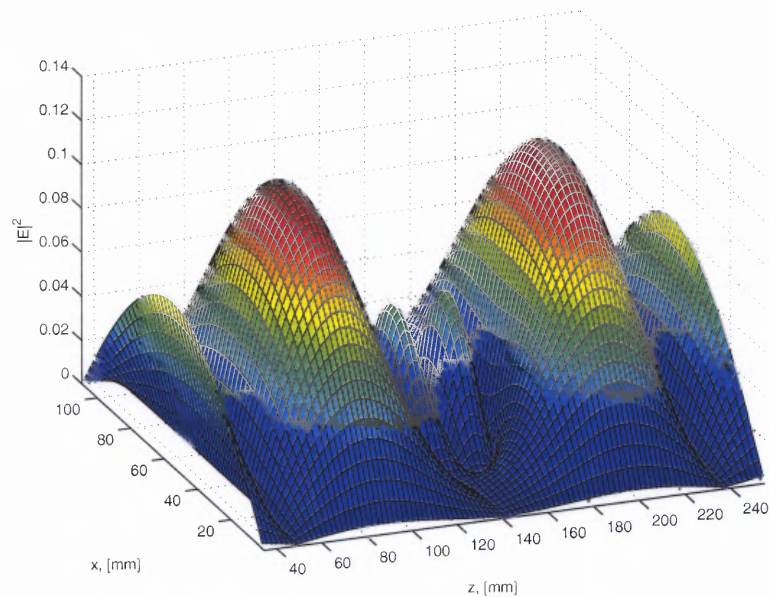
Figure 3.5 Magnitude of electric field inside a cavity when $|\rho_i|^2$ is at its maximum. The center of post locates at $x = 54.6$ mm and $z = 144.9$ mm.
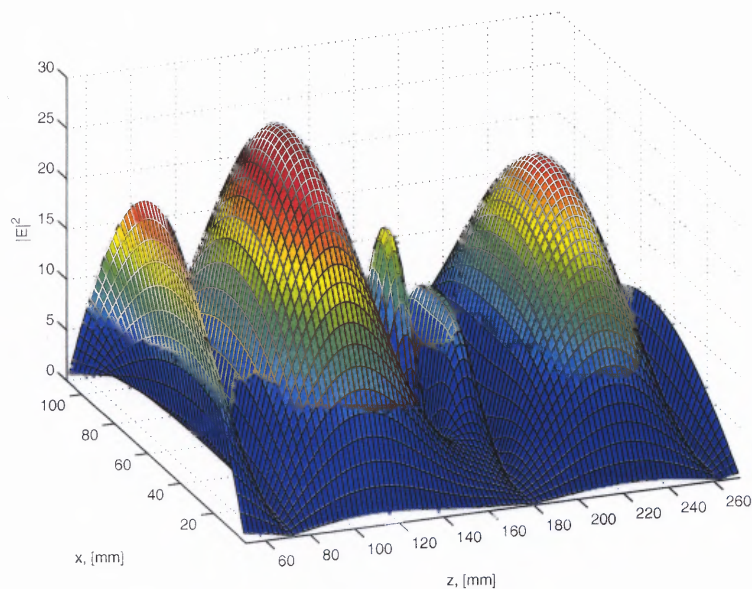
Figure 3.6 Magnitude of electric field inside a cavity when $|\rho_i|^2$ is at its minimum. The center of post locates at $x = 54.6$ mm and $z = 161.6$ mm.

CHAPTER 4

DISCRETIZATION OF HEAT EQUATION

We chose to use energy balance method [10] to discretize the heat equation because the energy balance method incorporates temperature dependence of thermal conductivity and boundary condition into the formulation much more elegant than discretization using numerical differentiation. It avoid differentiating thermal conductivity with respected to temperature explicitly. On the other hand, we have to numerically differentiate $\kappa \nabla T$. Similarly, we can discretize the Neumann's boundary condition without differentiation. However, it is possible to derive the same discretization as energy balance method using standard numerical differentiation. Figure (4.1a) shows

(a)   (b)
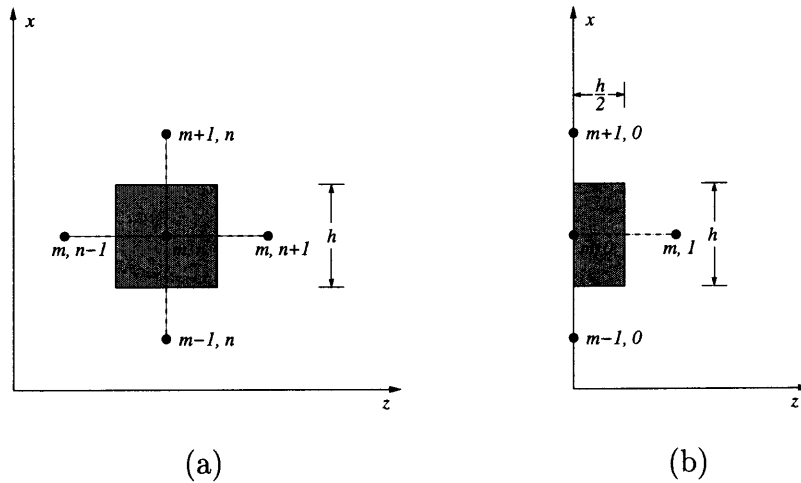
Figure 4.1 Control area (a) about an interior point, (b) about a point on the edge.

a five-point stencil with a control area centered at point (m, n). We know that the heat flow in an area is proportional to temperature gradient across its boundary. For the purpose of discretization, we assume the mesh size h is small enough to adequately approximate the temperature gradient by the ratio of differences, i.e.,

$$Q_{mn} = h\kappa \frac{T_{m+1n} - T_{mn}}{h} + h\kappa \frac{T_{m-1n} - T_{mn}}{h}$$

24

$$+ h\kappa \frac{T_{mn+1} - T_{mn}}{h} + h\kappa \frac{T_{mn-1} - T_{mn}}{h}.$$

$h\kappa$ measures the thermal conductance through the boundary. In the case where thermal conductivity varies with temperature, we use the temperature on the boundary, e.g. $\kappa\left(T_{m+\frac{1}{2}n}\right)$ or $\kappa_{m+\frac{1}{2}n}$ for short. The heat flow in a control area that is on the edge of the sample, we have to consider cooling effect by convection and radiation. Newton's law of cooling observes that heat flow in an area is proportional to temperature difference across the surface.

$$Q_{m0} = \frac{h}{2}\kappa \frac{T_{m+10} - T_{m0}}{h} + \frac{h}{2}\kappa \frac{T_{m-10} - T_{m0}}{h}$$
$$+ h\kappa \frac{T_{m1} - T_{m0}}{h} + h\eta\left(T_0 - T_{m0}\right) + h\varepsilon\left(T_0^4 - T_{m0}^4\right).$$

We denote the ambient temperature by T_0 and $\varepsilon = \mathcal{E}\varsigma$. The fourth power terms describe the radiation effect. Note that the one half factor on first two gradient terms is because the area is halved on the edge as shown in Figure (4.1b). Finally, heat flow inside an area is proportional to the rate of change of temperature. Including the heat source due to electrical resistance, we obtain the following discretization for interior mesh points.

$$h^2 \frac{T_{mn}^{j+1} - T_{mn}^j}{\Delta t} = \kappa_{m+\frac{1}{2}n}\left(T_{m+1n}^j - T_{mn}^j\right) + \kappa_{m-\frac{1}{2}n}\left(T_{m-1n}^j - T_{mn}^j\right)$$
$$+ \kappa_{mn+\frac{1}{2}}\left(T_{mn+1}^j - T_{mn}^j\right) + \kappa_{mn-\frac{1}{2}}\left(T_{mn-1}^j - T_{mn}^j\right)$$
$$+ h^2 \sigma_{mn} \left|\mathbf{E}\right|_{mn}^2,$$

where $\sigma_{mn} = \sigma\left(T_{mn}\right) \frac{t_{\text{diff}}}{t_{\text{oscill}}} \frac{\frac{\epsilon_0}{2}E_0^2}{\rho C_p T_0}$. For the numerical simulation, we choose a rectangular post for ease of implementation. Thus, discrete formulation for a mesh point along the edge of the sample except the corner is:

For $m = 0$ and $n = 1, \ldots, N - 1$,

$$\frac{h^2}{2}\frac{T_{0n}^{j+1} - T_{0n}^j}{\Delta t} = h\kappa_{\frac{1}{2}n}\frac{T_{1n}^j - T_{0n}^j}{h} + h\eta\left(1 - T_{0n}^j\right) + h\varepsilon\left(1 - T_{0n}^{j4}\right)$$

$$+ \frac{h}{2}\kappa_{0n+\frac{1}{2}}\frac{T_{0n+1}^{j} - T_{0n}^{j}}{h} + \frac{h}{2}\kappa_{0n-\frac{1}{2}}\frac{T_{0n-1}^{j} - T_{0n}^{j}}{h}$$

$$+ \frac{h^2}{2}\sigma_{0n}\left|\mathbf{E}\right|_{0n}^2 .$$

For $m = M$ and $n = 1, \ldots, N-1$,

$$\frac{h^2}{2}\frac{T_{Mn}^{j+1} - T_{Mn}^{j}}{\Delta t} = h\eta\left(1 - T_{Mn}^{j}\right) + h\varepsilon\left(1 - T_{Mn}^{j4}\right) + h\kappa_{M-\frac{1}{2}n}\frac{T_{M-1n}^{j} - T_{Mn}^{j}}{h}$$

$$+ \frac{h}{2}\kappa_{Mn+\frac{1}{2}}\frac{T_{Mn+1}^{j} - T_{Mn}^{j}}{h} + \frac{h}{2}\kappa_{Mn-\frac{1}{2}}\frac{T_{Mn-1}^{j} - T_{Mn}^{j}}{h}$$

$$+ \frac{h^2}{2}\sigma_{Mn}\left|\mathbf{E}\right|_{Mn}^2 .$$

For $n = 0$ and $m = 1, \ldots, M-1$,

$$\frac{h^2}{2}\frac{T_{m0}^{j+1} - T_{m0}^{j}}{\Delta t} = \frac{h}{2}\kappa_{m+\frac{1}{2}0}\frac{T_{m+10}^{j} - T_{m0}^{j}}{h} + \frac{h}{2}\kappa_{m-\frac{1}{2}0}\frac{T_{m-10}^{j} - T_{m0}^{j}}{h}$$

$$+ h\kappa_{m\frac{1}{2}}\frac{T_{m1}^{j} - T_{m0}^{j}}{h} + h\eta\left(1 - T_{m0}^{j}\right) + h\varepsilon\left(1 - T_{m0}^{j4}\right)$$

$$+ \frac{h^2}{2}\sigma_{m0}\left|\mathbf{E}\right|_{m0}^2 .$$

For $n = N$ and $m = 1, \ldots, M-1$,

$$\frac{h^2}{2}\frac{T_{mN}^{j+1} - T_{mN}^{j}}{\Delta t} = \frac{h}{2}\kappa_{m+\frac{1}{2}N}\frac{T_{m+1N}^{j} - T_{mN}^{j}}{h} + \frac{h}{2}\kappa_{m-\frac{1}{2}N}\frac{T_{m+1N}^{j} - T_{mN}^{j}}{h}$$

$$+ h\eta\left(1 - T_{mN}^{j}\right) + h\varepsilon\left(1 - T_{mN}^{j4}\right) + h\kappa_{mN-\frac{1}{2}}\frac{T_{mN-1}^{j} - T_{mN}^{j}}{h}$$

$$+ \frac{h^2}{2}\sigma_{mN}\left|\mathbf{E}\right|_{mN}^2 .$$

For the mesh point on the corners, the derivation is the same as the situation along the edge with an exception that the control area is one fourth of interior point's control area.

Corner $m = 0$ and $n = 0$,

$$\frac{h^2}{4}\frac{T_{00}^{j+1} - T_{00}^{j}}{\Delta t} = \frac{h}{2}\kappa_{\frac{1}{2}0}\frac{T_{10}^{j} - T_{00}^{j}}{h} + \frac{h}{2}\kappa_{0\frac{1}{2}}\frac{T_{01}^{j} - T_{00}^{j}}{h}$$

$$+ h\eta\left(1 - T_{00}^{j}\right) + h\varepsilon\left(1 - T_{00}^{j4}\right) + \frac{h^2}{4}\sigma_{00}\left|\mathbf{E}\right|_{00}^2 .$$

Corner $m = M$ and $n = 0$,

$$\frac{h^2}{4} \frac{T_{M0}^{j+1} - T_{M0}^{j}}{\Delta t} = \frac{h}{2} \kappa_{M-\frac{1}{2}0} \frac{T_{M-10}^{j} - T_{M0}^{j}}{h} + \frac{h}{2} \kappa_{M\frac{1}{2}} \frac{T_{M1}^{j} - T_{M0}^{j}}{h}$$
$$+ h\eta \left(1 - T_{M0}^{j}\right) + h\varepsilon \left(1 - T_{M0}^{j4}\right) + \frac{h^2}{4} \sigma_{M0} \left|\mathbf{E}\right|_{M0}^{2}.$$

Corner $m = 0$ and $n = N$,

$$\frac{h^2}{4} \frac{T_{0N}^{j+1} - T_{0N}^{j}}{\Delta t} = \frac{h}{2} \kappa_{\frac{1}{2}N} \frac{T_{1N}^{j} - T_{0N}^{j}}{h} + \frac{h}{2} \kappa_{0N-\frac{1}{2}} \frac{T_{0N-1}^{j} - T_{0N}^{j}}{h}$$
$$+ h\eta \left(1 - T_{0N}^{j}\right) + h\varepsilon \left(1 - T_{0N}^{j4}\right) + \frac{h^2}{4} \sigma_{0N} \left|\mathbf{E}\right|_{0N}^{2}.$$

Corner $m = M$ and $n = N$,

$$\frac{h^2}{4} \frac{T_{MN}^{j+1} - T_{MN}^{j}}{\Delta t} = \frac{h}{2} \kappa_{M-\frac{1}{2}N} \frac{T_{M-1N}^{j} - T_{MN}^{j}}{h} + \frac{h}{2} \kappa_{MN-\frac{1}{2}} \frac{T_{MN-1}^{j} - T_{MN}^{j}}{h}$$
$$+ h\eta \left(1 - T_{MN}^{j}\right) + h\varepsilon \left(1 - T_{MN}^{j4}\right) + \frac{h^2}{4} \sigma_{MN} \left|\mathbf{E}\right|_{MN}^{2}.$$

Since we do not know the temperature at half mesh points, we can only approximate the dimensionless thermal conductivity there. We can either approximate the thermal conductivity using known thermal conductivity values of surrounding mesh points or evaluate at an approximate temperature, i.e.,

$$\kappa_{m+\frac{1}{2}n} = \frac{1}{2} \left(\kappa_{mn} + \kappa_{m+1n}\right), \text{ or } \kappa_{m+\frac{1}{2}n} = \kappa \left(\frac{1}{2} \left(T_{mn} + T_{m+1n}\right)\right).$$

We can employ more points to get a more accurate average. We can solve the above discrete system either implicitly or explicitly. To solve the system implicitly, we have to assume that temperature dependence parameters like thermal and electric conductivities varies slowly with respected to temperature. Based on such assumption, we then linearize all the non-linear terms about previous time step. Let $\varphi(T)$ be the non-linear function of temperature, then φ at time step $j + 1$ is approximately,

$$\varphi\left(T^{j+1}\right) \approx \varphi\left(T^{j}\right) + \left.\frac{\partial \varphi}{\partial T}\right|^{j} \left(T^{j+1} - T^{j}\right),$$

where φ can be a conductance term $\kappa\left(T_{m+\frac{1}{2}n}^{j+1}\right)T_{mn}^{j+1}$, source term $\sigma\left(T_{mn}^{j+1}\right)|\mathbf{E}|_{mn}^{2}$, or radiation term $\left(T_{mn}^{j+1}\right)^{4}$. However, we will solve heat equation explicitly in favor of a simple implementation. As we mentioned in previous chapter, we do not consider temperature dependence of thermal conductivity in the numerical simulation in order to isolate the effect of the electrical conductivity. The general derivation is presented for completeness. Also, we note that the choice of implementation or temperature dependence of thermal conductivity does not affect the computational time significantly. The most time consuming process is computing the electric field which we discuss on the next chapter.

CHAPTER 5

DISCRETIZATION OF HELMHOLTZ EQUATION

5.1 Derivation of Discrete Equation

Using the centered difference scheme on a five-point stencil to discretize the Laplace's operator, we obtain a discrete representation of the Helmholtz's equation for all the interior points,

$$\left[4 - h^2 k^2(\epsilon_{mn} + i\sigma_{mn})\right] E_{mn} - E_{m+1n} - E_{m-1n} - E_{mn+1} - E_{mn-1} = 0, \qquad (5.1)$$

$$\text{for } m = 1, \ldots, M - 1; n = 1, \ldots, N - 1,$$

where M and N are the number of points along x- and z-axis, respectively, and h is spatial step size which equals to $\dfrac{1}{M}$. Since the electric field vanishes at the waveguide's walls,

$$E_{0n} = 0, \text{ and } E_{Mn} = 0. \qquad (5.2)$$

Suppose that there is no target; we can solve the difference equation (5.1) analytically with boundary condition (5.2). The solution is:

$$E_{mn} = e^{ik_z n} \sin\left(k_x m\right),$$

where $k_x = \dfrac{\pi}{M}$ and $k_z = \pm \cos^{-1}\left(2 - \dfrac{1}{2}h^2 k^2 - \cos\left(k_x\right)\right).$

Since it is a single mode waveguide, the field far from the target will exhibit a single propagating mode. With this knowledge, we put the target back into the problem and set the boundary conditions at $n = 0$ and $n = N$. Without loss of generality, there is an incident wave from the left, i.e. $e^{ik_z n} \sin\left(k_x m\right)$, scattered from the target. We expect that part of the wave will be reflected back and other will pass

by the target and propagate to the right end of the waveguide. Hence,

$$
E_{mn} = \begin{cases} \left(e^{ik_z n} + Re^{-ik_z n}\right) \sin\left(k_x m\right), & n \sim 0, \\[2mm] Te^{ik_z n} \sin\left(k_x m\right), & n \sim N. \end{cases}
$$

Thus, the boundary conditions at $n = 0$ and $n = N$ are:

$$
E_{m0} = (1 + R) \sin\left(k_x m\right) \quad \text{and} \quad E_{mN} = Te^{ik_z N} \sin\left(k_x m\right),
$$

where R and T are reflection and transmission coefficients, respectively. Since R and T are unknown, we can eliminate them by using the electric field at $n = 1$ and $n = N - 1$, i.e.

$$
E_{m1} = \left(e^{ik_z} + Re^{-ik_z}\right) \sin\left(k_x m\right),
$$

$$
\text{and} \quad E_{mN-1} = Te^{ik_z(N-1)} \sin\left(k_x m\right).
$$

Combining with the boundary conditions at $n = 0$ and $n = N$, we have

$$
E_{m0} = e^{ik_z} E_{m1} + \left(1 - e^{2ik_z}\right) \sin\left(k_x m\right),
$$

$$
\text{and} \quad E_{mN} = e^{ik_z} E_{mN-1}.
$$

These are exact non-reflecting boundary conditions for the propagating mode of the discrete equations. They ensure that no artificial reflection introduced into the computational domain by the numerical method. Hence, the difference equation for $n = 1$ and $n = N - 1$ are,

$$
\left[4 - h^2 k^2 - e^{ik_z}\right] E_{m1} - E_{m+11} - E_{m-11} - E_{m2} = \left(1 - e^{2ik_z}\right) \sin\left(k_x m\right),
$$

$$
\text{and} \quad \left[4 - h^2 k^2 - e^{ik_z}\right] E_{mN-1} - E_{m+1N-1} - E_{m-1N-1} - E_{mN} - E_{mN-2} = 0,
$$

provided the target is not near the boundaries $n = 0$ and $n = N$; therefore, $\epsilon_{m1} = \epsilon_{mN} = 1$ and $\sigma_{m1} = \sigma_{mN} = 0$.

5.2 Structure of Discrete Equations

We rewrite the difference equations as a system of linear equations $Lu = f$, where

$$
L = \begin{pmatrix} L_1 & -I_{M-1} & & O_{M-1} \\ -I_{M-1} & L_2 & \ddots & \\ & \ddots & \ddots & -I_{M-1} \\ O_{M-1} & & -I_{M-1} & L_{N-1} \end{pmatrix}, \quad u = \begin{pmatrix} u_1 \\ u_2 \\ \vdots \\ u_{N-1} \end{pmatrix}, \quad f = \begin{pmatrix} f_1 \\ f_2 \\ \vdots \\ f_{N-1} \end{pmatrix},
$$

$$
L_n = \begin{pmatrix} l_{1n} & -1 & & 0 \\ -1 & l_{2n} & \ddots & \\ & \ddots & \ddots & -1 \\ 0 & & -1 & l_{M-1n} \end{pmatrix}, \quad u_n = \begin{pmatrix} E_{1n} \\ E_{2n} \\ \vdots \\ E_{M-1n} \end{pmatrix},
$$

$$
l_{mn} = \begin{cases} 4 - h^2 k^2 - e^{ik_z}, & n = 1, N - 1, \\ 4 - h^2 k^2 \left(\epsilon_{mn} + i\sigma_{mn} \right), & n = 2, \ldots, N - 2. \end{cases}
$$

$$
f_n = \begin{cases} (1 - e^{2ik_z}) \sin(k_x m), & n = 1, \\ 0, & n = 2, \ldots, N - 1, \end{cases}
$$

where I_m is the identity matrix of order m and O_m is the zero matrix of order m. As we can see the information about boundary conditions of the truncated ends of the waveguide is encoded in L_1, L_{N-1} and f_1, while the information about the target is scattered in a few other L_n's due to the small size of the target.

5.3 Splitting Discrete Operator for Numerical Solution

It is impractical to directly invert L due its large scale. However, we can invert the matrix by taking advantage of its structure. By the choice of stencil, L is a very sparse matrix. And, it is almost symmetric because of the symmetry of the Laplacian and the use of centered difference scheme. Therefore, we can decompose L into the symmetric part and non-symmetric part. We then apply the conjugate gradient method to solve the symmetric part. The non-symmetric part encodes information

about the truncated ends of waveguide and the target. Since the size of the target is small compared to the width of the waveguide, the non-symmetric part is a low rank matrix. With some algebraic manipulation, we can invert L by inverting a sparse and symmetric matrix and a low-rank matrix.

$$L = A + B + C, \tag{5.3}$$

where A is a symmetric matrix that contains no information about target or boundary conditions, B stores the information of the boundary conditions, and the diagonal matrix C contains information of the target. Hence, A will have the same structure as L except with constant diagonal elements, i.e., $a_{ii} = 4 - h^2 k^2$. B and C have the following form:

$$B = \begin{pmatrix} B_1 & & O_{M-1} \\ & O_{M-1} & \\ O_{M-1} & & B_{N-1} \end{pmatrix}, \quad B_1 = B_{N-1} = -e^{ik_z} I_{M-1},$$

$$\text{and} \quad c_{jj} = \begin{cases} -h^2 k^2 \left(\epsilon_{mn} + i\sigma_{mn} + 1 \right), & (m,n) \in \text{target}, \\ 0, & \text{otherwise}. \end{cases}$$

The rank of B is $2(M-1)$ and the rank of C is the number of discretization points of the target which is small comparing to the total number of discretization points MN. Since B and C are not full rank matrices, their sum can be expressed as the product of MN-by-P matrix Q and P-by-MN matrix S, where P is sum of $2(M-1)$ and number of grid point in the target. Thus, the linear system becomes,

$$Au + QSu = f$$

We can solve for u as follow. Because A is a sparse matrix, we use the conjugate gradient method to solve systems with A as their matrix. We apply the method to each column of Q. However, A is not a positive definite matrix for certain range of

k, and we will address this later.

$$u + A^{-1}QSu = A^{-1}f.$$

Then, we solve for Su,

$$Su + SA^{-1}QSu = SA^{-1}f,$$

$$Su = \left(I + SA^{-1}Q\right)^{-1} SA^{-1}f.$$

The dimension of $SA^{-1}Q$ is the same as the rank of Q or S which is small in comparison to the rank of A. Therefore, we use Gaussian elimination to invert $I + SA^{-1}Q$. Thus,

$$u = A^{-1}f - A^{-1}Q\left(I + SA^{-1}Q\right)^{-1} SA^{-1}f. \qquad (5.4)$$

In practice, we expect to solve equation (5.4) repeatedly when the electrical conductivity σ depends on temperature. However, we can avoid redundant computation by put all the temperature dependence on S, and Q is left with only 0's and 1's as its entries. Although we, in theory, do not to have recompute $A^{-1}Q$ when temperature varies, it requires enormous amount of storage to save $A^{-1}Q$ for reuse. Fortunately, Q^{T} has the same structure as S by construction. Thus, $Q^{\mathrm{T}}A^{-1}Q$ stores enough information to compute $SA^{-1}Q$ and requires much less storage than $A^{-1}Q$. As a result, we are able to separate the temperature independence $Q^{\mathrm{T}}A^{-1}Q$ from the temperature dependence S.

5.4 Handling Negative Eigenvalues

When $k = 0$, the matrix A in the equation (5.3) corresponds to the discretization of Laplace's operator on a rectangular domain with Dirichlet boundary conditions. Let A_0 be A when $k = 0$. A_0 is a positive definite matrix; hence, we can use conjugate

gradient method to solve the system,

$$A_0 x = b.$$

If we perturb A_0 by $-\delta I$, the eigenvalues of A_0 are shifted to the left for positive δ. For large enough δ, some of the eigenvalues of $A_0 - \delta I$ will be negative, and the conjugate gradient method fails. However, we still can invert $A_0 - \delta I$ using conjugate gradient method indirectly.

Suppose there are small number of α's eigenvalues of A_0 less than or equal to δ. Rewriting the system $(A_0 - \delta I) x = b$ as follow:

$$\left(A_0 - \delta I + p\delta \sum_\alpha v_\alpha v_\alpha^{\mathrm{T}} - p\delta \sum_\alpha v_\alpha v_\alpha^{\mathrm{T}} \right) x = b,$$

where v_α are eigenvectors corresponding to those α's eigenvalues. Or, in the matrix form,

$$\left(A_0 - \delta I + p\delta V V^{\mathrm{T}} - p\delta V V^{\mathrm{T}} \right) x = b, \tag{5.5}$$

where $V = (v_1 \, v_2 \cdots v_\alpha)$. For any $p > 1$, the matrix $\Delta = A_0 - \delta I + p\delta V V^{\mathrm{T}}$ is positive definite; therefore, we can use conjugate gradient on Δ. As before, we take advantage of low rank matrices, we can invert A by following the above procedure of computing u. Replacing x, Δ, b, V, and $-p\delta V^{\mathrm{T}}$ for u, A, f, Q and S in equation (5.4), respectively. We have,

$$x = \Delta^{-1} b + p\delta \Delta^{-1} V \left(I - p\delta V^{\mathrm{T}} \Delta^{-1} V \right)^{-1} V^{\mathrm{T}} \Delta^{-1} b.$$

Since the columns of V are eigenvectors of Δ, we can simplify the above expression further. First, we express Δ^{-1} in its diagonalized form; however, we retain $\Delta^{-1} b$ because it is the result of conjugate gradient method.

$$\Delta^{-1} = \Gamma \Lambda^{-1} \Gamma^{\mathrm{T}}.$$

Expressing Γ as $(V\ W)$. V is the same matrix as in equation (5.5); hence, W contains eigenvectors corresponding with eigenvalues of A_0 that are greater than δ.

$$
\Delta^{-1} = \begin{pmatrix} V & W \end{pmatrix} \begin{pmatrix} \Lambda_\alpha^{-1} & O_{\alpha\beta} \\ O_{\beta\alpha} & \Lambda_\beta^{-1} \end{pmatrix} \begin{pmatrix} V^{\mathrm{T}} \\ W^{\mathrm{T}} \end{pmatrix},
$$

where $\Lambda_\alpha = \mathrm{diag}\,(\lambda_\alpha + (p-1)\delta)$ and $\Lambda_\beta = \mathrm{diag}\,(\lambda_\beta - \delta)$. Multiplying by V to both sides of the equation,

$$
\begin{aligned}
\Delta^{-1}V &= \begin{pmatrix} V & W \end{pmatrix} \begin{pmatrix} \Lambda_\alpha^{-1} & O_{\alpha\beta} \\ O_{\beta\alpha} & \Lambda_\beta^{-1} \end{pmatrix} \begin{pmatrix} V^{\mathrm{T}} \\ W^{\mathrm{T}} \end{pmatrix} V \\
&= \begin{pmatrix} V & W \end{pmatrix} \begin{pmatrix} \Lambda_\alpha^{-1} & O_{\alpha\beta} \\ O_{\beta\alpha} & \Lambda_\beta^{-1} \end{pmatrix} \begin{pmatrix} I_\alpha \\ O_{\beta\alpha} \end{pmatrix} \\
&= \begin{pmatrix} V & W \end{pmatrix} \begin{pmatrix} \Lambda_\alpha^{-1} \\ O_{\beta\alpha} \end{pmatrix} \\
&= V\Lambda_\alpha^{-1}
\end{aligned}
$$

Using the above equality, we can simplify other expressions such as,

$$
I - p\delta V^{\mathrm{T}}\Delta^{-1}V = \mathrm{diag}\left(\frac{\lambda_\alpha - \delta}{\lambda_\alpha + (p-1)\delta}\right),
$$

and ultimately,

$$
x = \Delta^{-1}b + V\,\mathrm{diag}\left(\frac{p\delta}{\lambda_\alpha - \delta}\right) V^{\mathrm{T}}\Delta^{-1}b.
$$

From the above expression, we can see that the modified method fails only when δ is an eigenvalue of A_0.

Since A_0 is the discretization of Laplace's operator, we know what its eigenvalues and eigenvectors are,

$$
\lambda^{(\mu\nu)} = 4 - 2\cos\left(\frac{\mu\pi}{M}\right) - 2\cos\left(\frac{\nu\pi}{N}\right), \tag{5.6}
$$

$$v_{mn}^{(\mu\nu)} = \frac{2}{\sqrt{MN}} \sin\left(\frac{\mu\pi m}{M}\right) \sin\left(\frac{\nu\pi n}{N}\right), \tag{5.7}$$

where $m,\mu = 1,\ldots,M-1$, and $n,\nu = 1,\ldots,N-1$. If we set $\delta = h^2 k^2$, $A_0 - \delta I$ becomes A in equation (5.3). Therefore, for an given k, we know how many negative eigenvalues A has, and modify the conjugate gradient method with appropriate V.

By inspecting the eigenvalues in equation (5.6), we note that the spectral condition number,

$$\kappa_2(A_0) = \frac{\lambda_{\max}}{\lambda_{\min}} = \frac{4 - 2\cos\left(\frac{(M-1)\pi}{M}\right) - 2\cos\left(\frac{(N-1)\pi}{N}\right)}{4 - 2\cos\left(\frac{\pi}{M}\right) - 2\cos\left(\frac{\pi}{N}\right)},$$

grows because $\lambda_{\min}$ tends to zero as M and N increase. Since the convergence rate of the conjugate gradient method is $\frac{\sqrt{\kappa_2}-1}{\sqrt{\kappa_2}+1}$ [11], which is linear for large spectral condition number κ_2. Therefore, we expect the conjugate gradient method converges slowly as M and N increase.

5.5   Fast Sine Transform

Alternatively, we can solve the system $Ax = b$ by the method of fast sine transform. Since the matrix A shares the same set of eigenvectors (5.7) as A_0, we can diagonalize A as,

$$A = \Gamma D \Gamma, \quad D = \text{diag}\left(\lambda^{(\mu\nu)} - h^2 k^2\right), \quad \text{and} \quad \Gamma = \left(v_{mn}^{(\mu\nu)}\right).$$

Hence,

$$x = \Gamma D^{-1} \Gamma b.$$

Each multiplication by Γ can be achieved quickly by a fast sine transform. We use the fast sine transform from FFTW package, which stands for Fastest Fourier Transform in the West, developed by Frigo and Johnson of MIT [12].

CHAPTER 6

NUMERICAL TESTS

Our numerical method is based on splitting the discrete operator L into $A + QS$. The analysis from previous section has demonstrated that we can find the field inside an infinite waveguide with the presence of an obstacle, i.e.,

$$u = A^{-1}f - A^{-1}Q \left(I + SA^{-1}Q\right)^{-1} SA^{-1}f.$$

It is clear from the analysis, that A is invertible provided that none of its eigenvalues equals to $h^2 k^2$. However, it is unclear that the matrix $I + SA^{-1}Q$ is invertible. We believe that the solution u existed because the system is the discretization of a well-posed continuous problem. Therefore, the purpose of this section is to provide a definite confirmation that the numerical method does what we expect it to do. We will perform three tests in which we know either the field or some quantity that can check against the numerical result. The first of such tests is determining the electric field inside an empty infinite single mode waveguide with the disturbance of unit strength starting at negative infinity. We know the solution to the difference equations is $e^{ik_z n} \sin\left(k_x m\right)$ which is the discrete version of the right-traveling wave. However, the problem is viewed differently to the method; it is finding the field inside an infinite waveguide with an obstacle of size zero. So, S only contains the information at boundaries of the truncated waveguide, and their ranks reduce to $2(M - 1)$. Figure (6.1) shows the real and imaginary parts of the electric fields computed for a truncated waveguide of 109.22 mm in width and 222.9 mm in length. The grid size h is 1.11 mm which corresponds to M = 98 and N = 200. The disturbance frequency is 2.45 GHz, and the center of the sample is at $z = 0$. As we can see, the field is simply a cosine or sine wave. More evidently, the magnitude of the
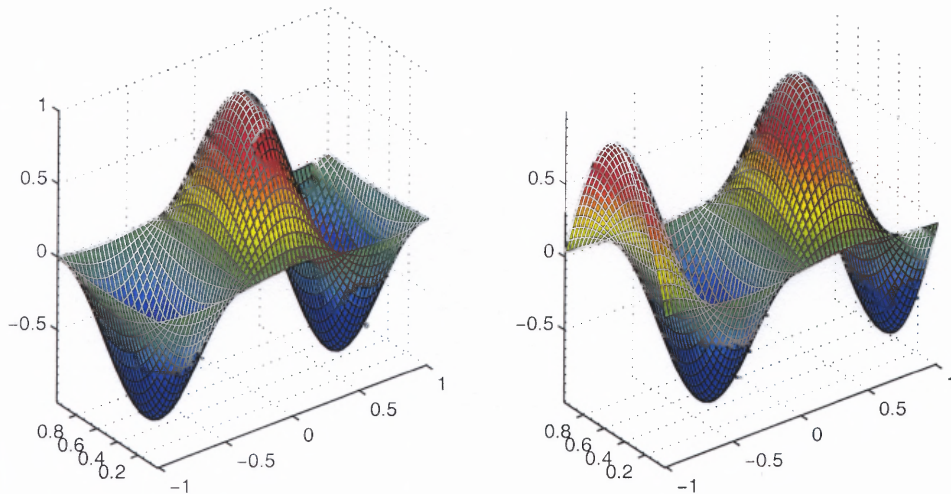
Figure 6.1 Real and imaginary parts of electric field inside an infinite empty waveguide.

electric field is $\sin(k_x m)$ as show in Figure (6.2). We can further verify the numerical method by checking various quantities such as wavelength, reflection and transmission coefficients, etc. Figure (6.3) shows that the wavelength of the numerical solution is about 147.11 mm as comparison to the exact discrete wavelength $\dfrac{2\pi h}{k_z} = 148.02$ which is accurate to the order of grid size h. Since it is an empty waveguide, we expect that there is no reflection; hence reflection coefficient is zero and transmission coefficient is one. The numerical reflection and transmission coefficients are accurate to the order 10^{-13}.

The second test is determining the electric field inside infinite single mode waveguide in presence of a transparent square post; i.e. the post has the same properties as its surrounding. Since the post is fictitious, the field is the same as the case of empty waveguide. Suppose the incident wave of unit strength emerges from negative infinity, then the field is simply a right-traveling wave, $e^{ik_z n} \sin(k_x m)$. Similar to the first test, the method does not realize the waveguide is empty; it stores in S the information at boundaries of the truncated waveguide and the properties of the post. The fields in Figure (6.4) is computed using the same set of parameters
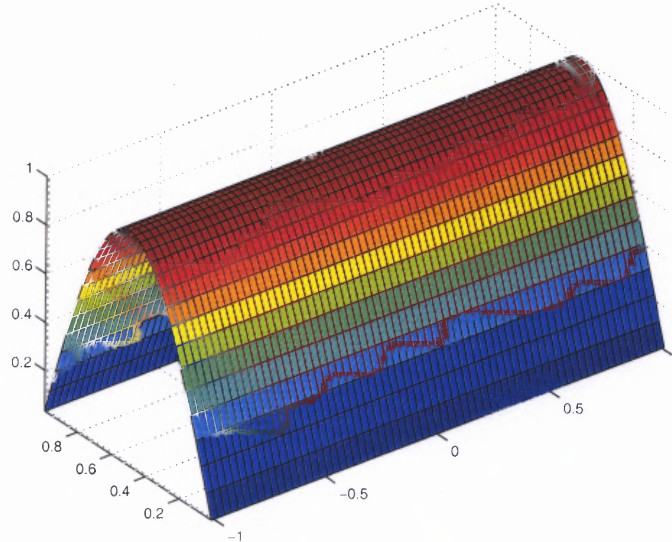
Figure 6.2   Magnitude of the electric field inside an empty waveguide

as the first test with the exception of the size of the post and its properties. The post measures 41.07 mm by 41.07 mm, and its relative permittivity is one and its effective conductivity is set to zero. As expected, the numerical results are the same for both tests as shown Figure (6.1) and (6.4). The numerical wavelength, reflection and transmission coefficients are computed with similar accuracy as the first test.

Another test that we can perform that has the exact solution is a slab of constant electrical conductivity inside an infinite waveguide. We can solve this problem exactly by applying the continuity of electric field and its derivative at the interfaces of the slab. In this test, a slab of thickness 21.2 mm whose center is placed at $z = 111.4$ mm. The slab has a constant electrical conductivity of 5×10^{-4} $\Omega^{-1}\mathrm{m}^{-1}$ and dielectric constant of 9.7. The rest of the parameters such waveguide dimensions and microwave frequency are the same as previous tests. Figure (6.5) plots the magnitude of the dimensionless electric field which is accurate to the order 10^{-3}. The absolute error through the centerline $x = 54.6$ mm is shown in Figure (6.6).
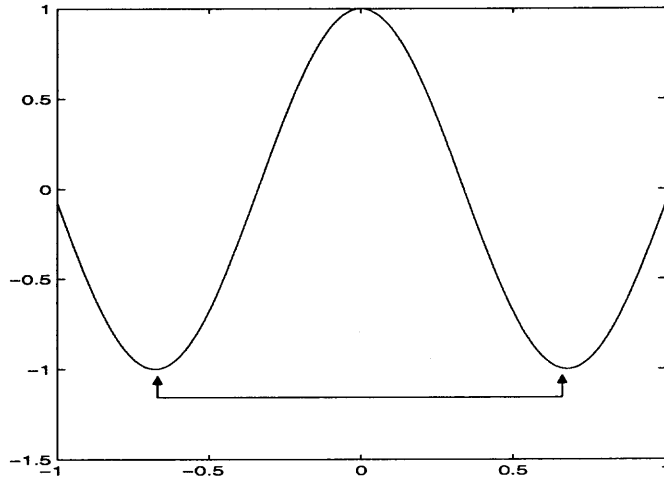
Figure 6.3 The cross-section of the real part of electric field along the centerline $x = 54.6$ mm.

The setup for the final test is an infinite waveguide in presence of a lossless square post. There is no simple expression for the field in this case, so we can not really check the solution by investigating the graph of the solution, or the reflection coefficient, etc. Instead, we verify other quantities that always true for certain set of parameters. For example, the conservation of power for lossless material.

$$|R|^2 + |T|^2 = 1, \text{ and } RT^* + TR^* = 0. \tag{6.1}$$

The equation (6.1) is derived in §A.2. We use the same setting as the second test with 9.7 as the relative permittivity. The numerical reflection and transmission coefficients satisfies equation (6.1) to the order of 10^{-6} accuracy. Based on the result of those four tests, we are confident that our numerical method computes what we expect it to.
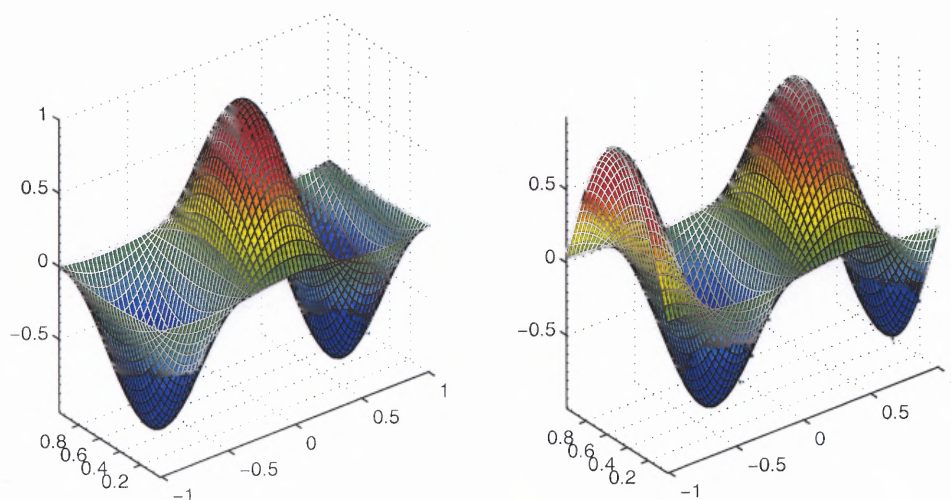
Figure 6.4 Real and imaginary parts of electric field inside an infinite waveguide in presence of a 41.07-mm square post with unity relative permittivity ($\epsilon = 1$) and zero effective conductivity ($\sigma = 0$).
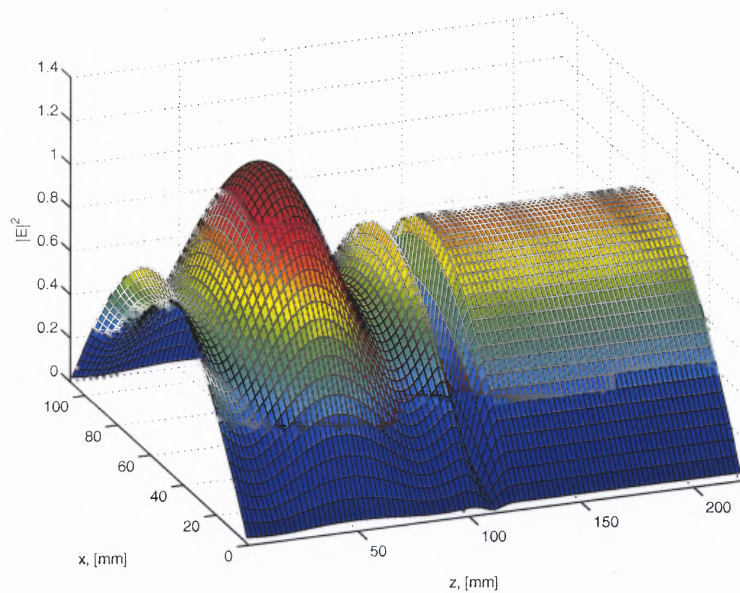

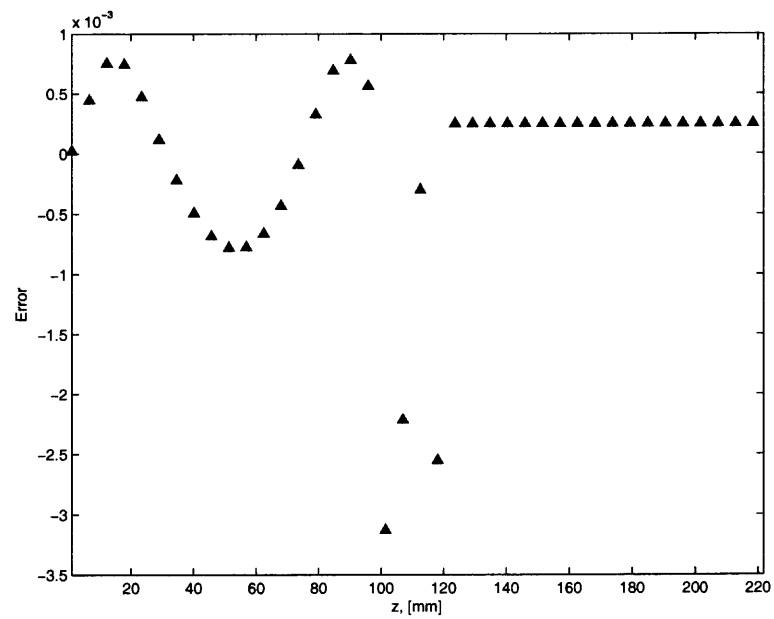**Figure 6.5** Magnitude of the electric field inside an infinite waveguide in presence of a 21.2-mm slab.

Figure 6.6 Absolute error of the magnitude of electric field along the centerline $x = 54.6$ mm.

CHAPTER 7

NUMERICAL RESULTS

For the heating problem we using the following set of physical parameters [10, 13, 14, 15]:

Parameters	Values
Aperture size, $W - 2A$	17.48 mm
Dielectric constant, ϵ	9.7
Emissivity, $\mathcal{E}$	0.87
Heat transfer coefficient, η	15 W/m^2 K
Input power, P	1000 W
Mass density, ρ	2000 kg/m^3
Microwave frequency, $\omega/2\pi$	2.45 GHz
Specific heat, C_p	600 J/kg K
Thermal conductivity, κ_0	120 W/m K
Waveguide width, W	109.22 mm

For these particular values, the diffusion time $t_{\text{diff}} = \dfrac{\rho C_p W^2}{\kappa_0}$ works out to be 119.3 seconds. As before, we lay a grid of size 1.11 mm on the truncated waveguide with $M = 98$ and $N = 200$. We choose sufficiently small $\Delta t = \dfrac{h^2}{8}$, which is roughly 1.56 milliseconds per time step, to avoid the numerical instability. We then attempt to heat a square post of size 40.1 mm whose center locates at $x = 54.6$ mm and $z = 144.9$ mm by exciting the cavity with an electric field of magnitude $E_0 = 1.75 \times 10^4$ Vm^{-1}. We designate three different profiles for the electrical conductivity of the post. Two electrical conductivity profiles are constant with $\sigma = 10^{-4}\Omega^{-1}\text{m}^{-1}$ and $4 \times 10^{-4}\Omega^{-1}\text{m}^{-1}$. For comparison, the third profile is a linear function of temperature

which has value of $4 \times 10^{-5}\Omega^{-1}\mathrm{m}^{-1}$ at 20°C and $5 \times 10^{-4}\Omega^{-1}\mathrm{m}^{-1}$ at 1000°C. The profiles are shown in Figure (7.1). The numerical simulations run for those three
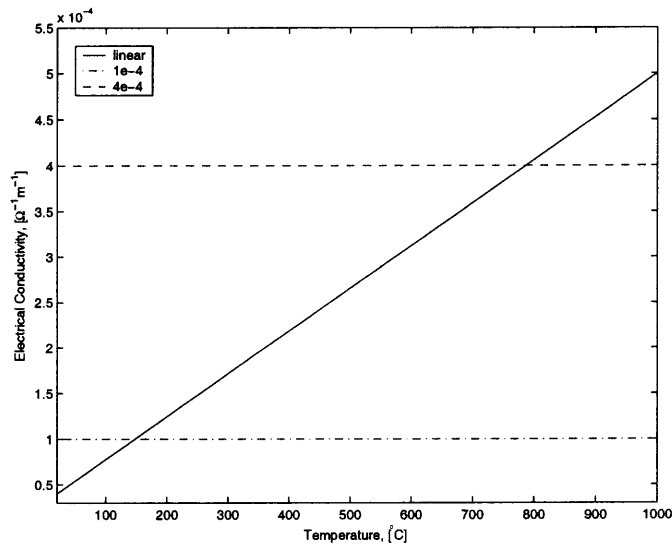

Figure 7.1 The electrical conductivity profiles.

profiles until the temperature inside the post reach the equilibrium. For the constant profiles, the electric field is computed only one and used for the entire heating process. On the other hand, temperature dependent profile requires constantly updating of the electric field. In order to obtain the result within a reasonable time, we decide to update the electric field every 10°C in temperature variation. The temperature history is recorded at every thousand time steps. Figures (7.2)–(7.4) plot the equilibrium temperature distributions inside the sample. At first look, three temperature distributions are qualitatively the same. Upon close inspection, we see that there are noticeable differences. The most obvious difference is the temperature variation among the figures. The temperature distribution corresponding with $\sigma = 4 \times 10^{-4}$ attains the highest maximum in all three at 1167.8°C. On the other hand, the simulation associates with linearly varying σ reaches its equilibrium in the shortest time. The temperature gradient for all three distributions is about 50°C. Figures (7.5) and (7.6) show the temperature history at the center and one of the corner. There
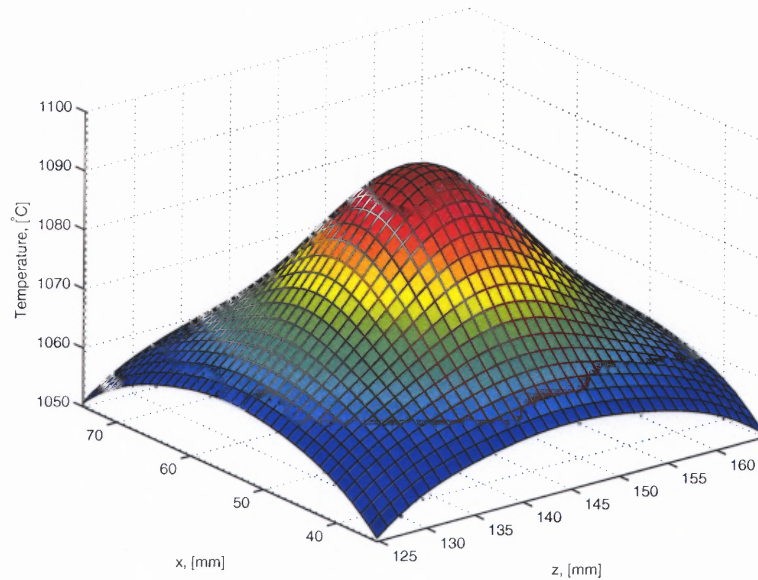
Figure 7.2 Equilibrium temperature distribution for
$\sigma = 10^{-4}$. The simulation reaches steady state around
132000 time steps which is about 3.42 min.

is not much different between two graphs besides the obvious temperature difference.
The corners and edges are cooler than the interior is simply the consequence of
cooling effect on the surface. We note the temperature of linear profile overtakes the
temperature corresponding to $\sigma = 10^{-4}$. This is the result of two profiles intersect
as show in Figure (7.1). However, there is a delay for the temperature to build up
which may explain why the second intersection never occurs.

Those simulations requires storage of 60 MB and solving a 1600-by-1600 system
of equations. A Sun's 400 MHz Ultra 5 workstation takes about a minute of its CPU
time to solve 1600-by-1600 system of equations. Hence, it would take about two hours
to simulate the above heating process for the case of linear conductivity profile.

Since we want to optimize the energy deposition into the sample, we dynamically
adjust the cavity length when we recompute the electric field. However, we learn that
the variation of the electrical conductivity σ has little effect on the optimal length.
Figure (7.7) shows the absorption power of a square post of size 40.1 mm, whose
center locates at $x = 54.6$ mm and $z = 144.9$ mm, for different values of σ. The blue
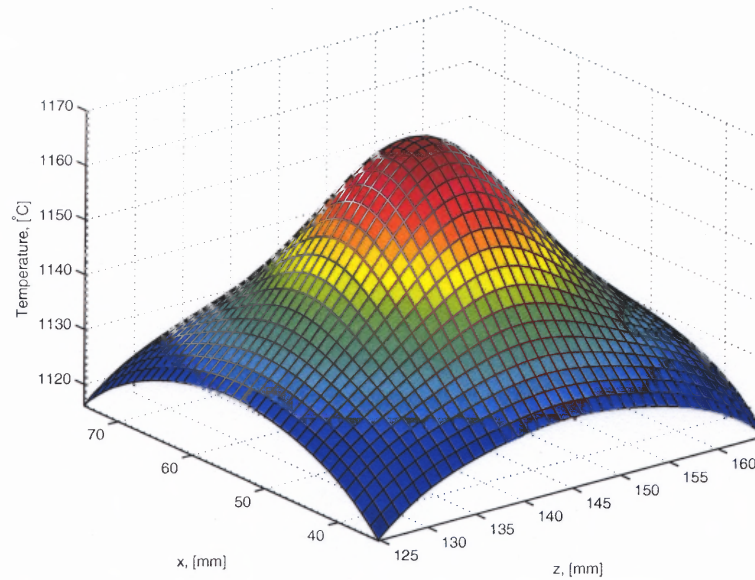
Figure 7.3 Equilibrium temperature distribution for $\sigma = 4 \times 10^{-4}$. The simulation reaches steady state around 119000 time steps which is about 3.08 min.

triangle represents the absorption power at the optimal length while the red triangle is the absorption power at the optimal length of $\sigma = 0$. The absolute error in absorption power and optimal length are shown in Figures (7.8) and (7.9), respectively. As we can see, the error in power absorption is on the order of 10^{-2} W, and the difference in optimal length is on the order of 10^{-2} mm. These differences are small comparing to the absorption power of 100 W and optimal length of 260 mm. We also find that the placement of the sample significantly effects the absorption power and optimal length. The absorption power and optimal length for two different locations of a sample are shown in Figures (7.10) and (7.11), respectively. The blue triangles are the results of the same settings as before. The red triangles are the results of moving the sample 22.3 mm along the cavity.
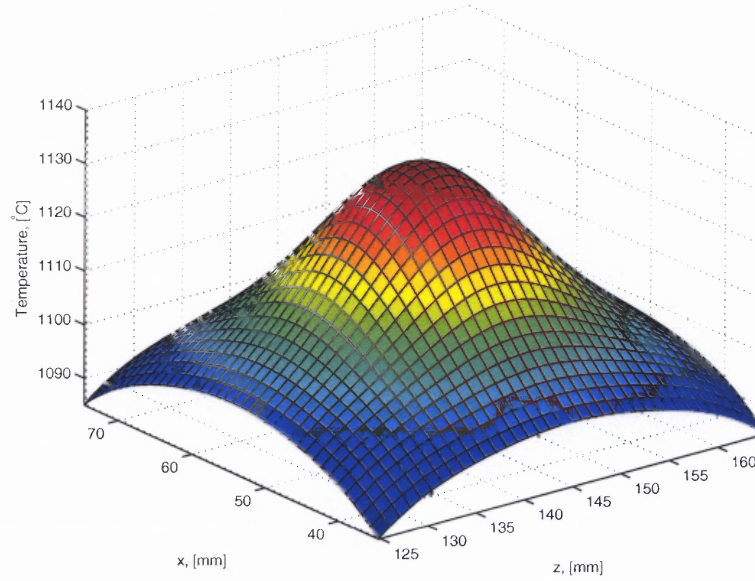
Figure 7.4 Equilibrium temperature distribution where σ is linear function of temperature. The simulation reaches steady state around 115000 time steps which is about 2.98 min.
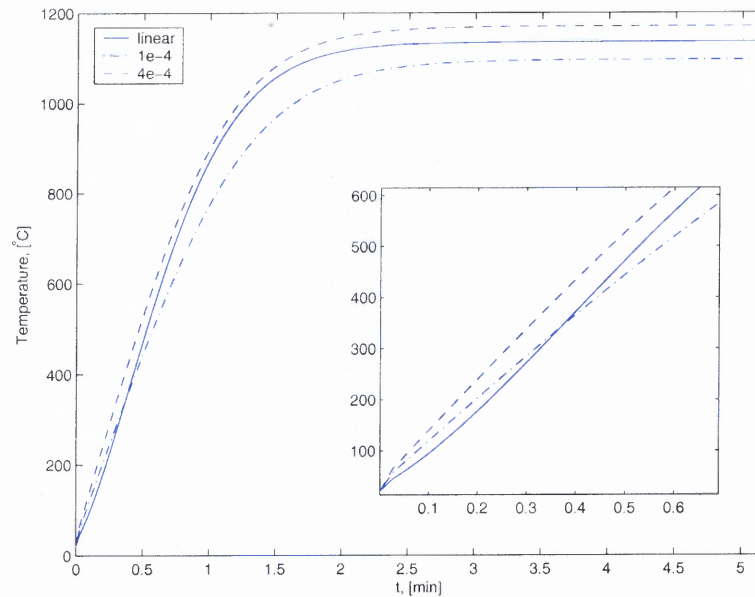

Figure 7.5 Temperature history of the sample's center for three different σ profiles.

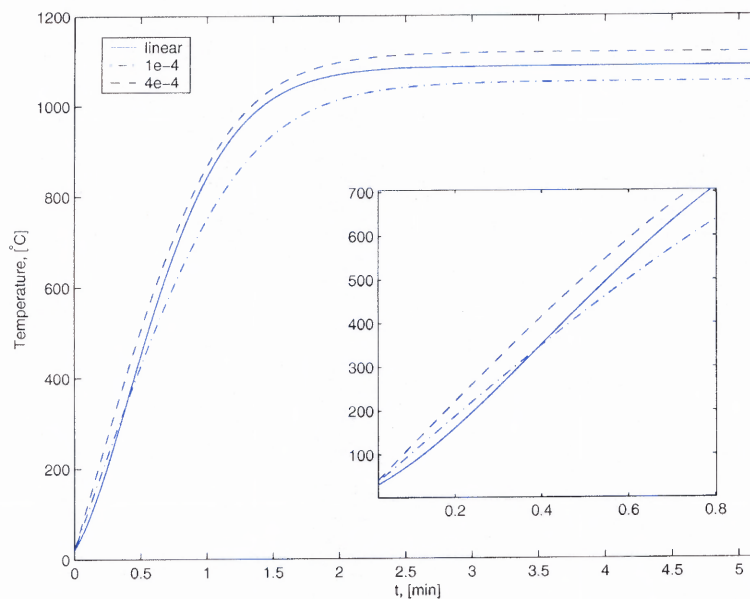**Figure 7.6** Temperature history of one of the corners of the sample for three different σ profiles.
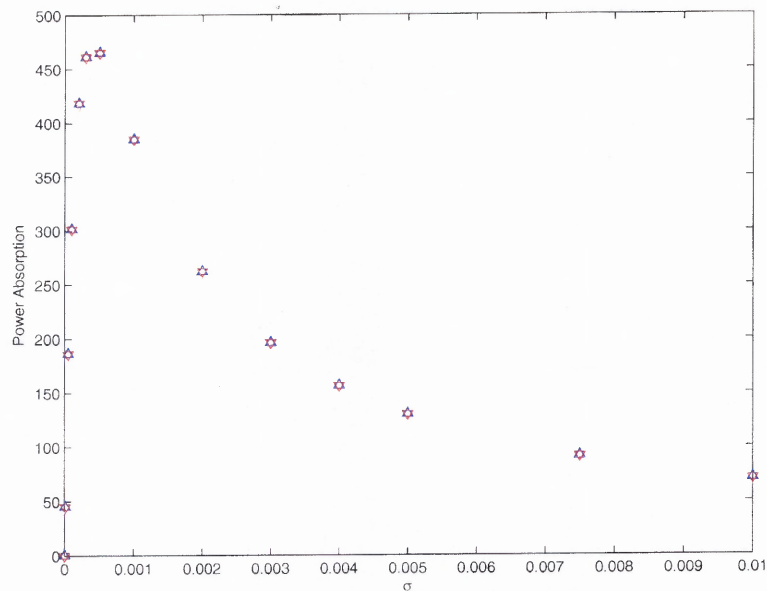

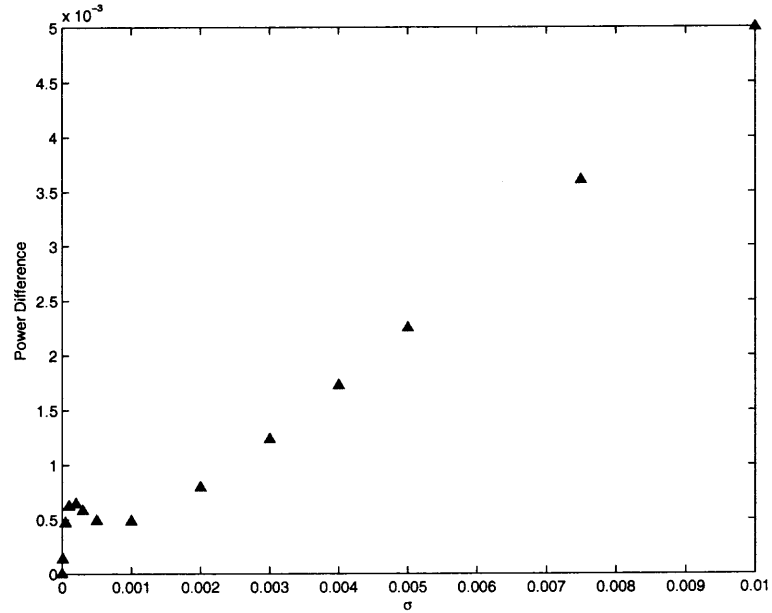**Figure 7.7** Power absorption by the sample.

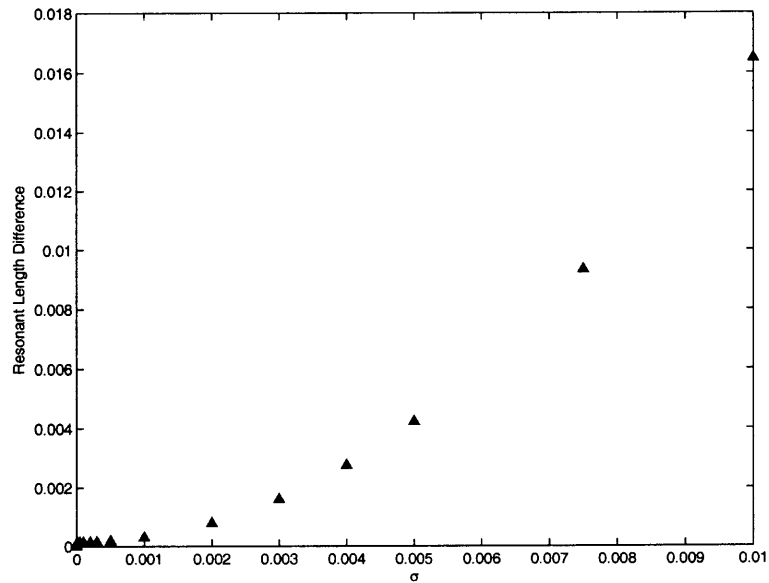**Figure 7.8** Absorption power difference for different optimal lengths.

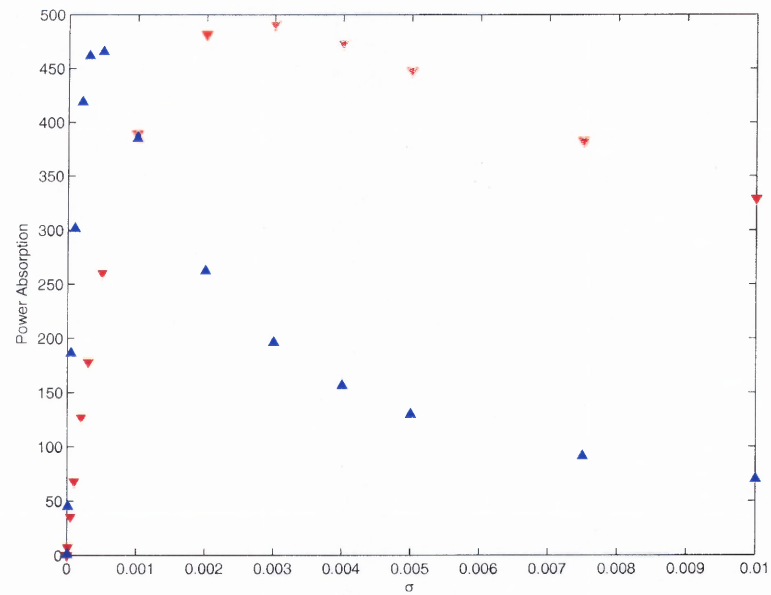
Figure 7.9 Difference in optimal length.

Figure 7.10 Absorption power for different locations of a sample.
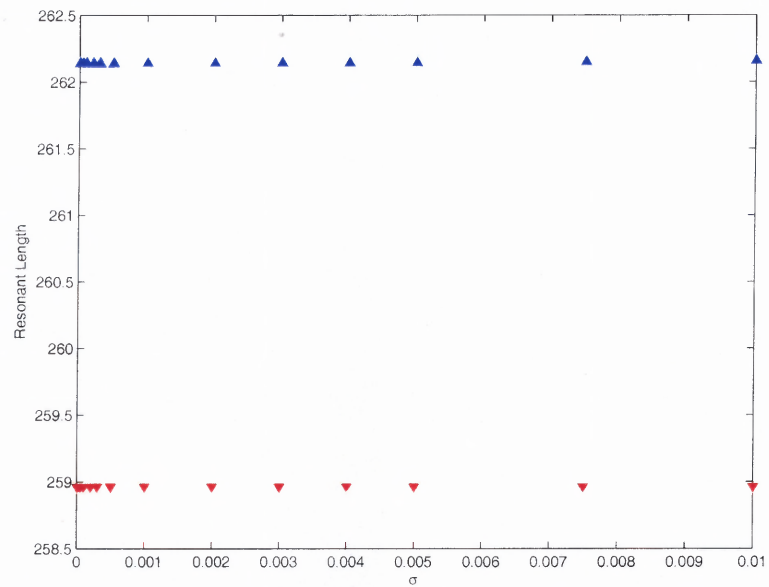

Figure 7.11 Optimal length for different locations of a sample.

CHAPTER 8

CONCLUSIONS

It is impractical, if not impossible, to numerically simulate the coupled Maxwell's equations (3.1) and heat equation (3.2) because of the vast difference in scales of the electromagnetic oscillation time and thermal conducting time. The electromagnetic fields oscillate about a million times faster than it takes heat to spread across the sample. Therefore, the direct simulation would march millions of time steps in order to observe any temperature variation and sufficiently capture the behavior of the electromagnetic fields. As a consequence, time-average heat equation (3.5) is always used in place of equation (3.2). It waits for the transient electromagnetic disturbance to radiate out of the computational domain before marching to the next time step in the heat equation. FDTD is often employed as a solver in determining the harmonic steady state electromagnetic fields. Note that the number of time steps FDTD takes until the steady state emerges is not related to the time step of the heat equation. From the perspective of the heat equation, the change in electromagnetic field is instantaneous. In this dissertation, we determine the electric field by solving the Helmholtz equation with a finite-difference method. This direct approach has its advantage. The time-harmonic steady state electric field can be found without time-stepping; there is no concern with transient disturbances radiating out of the computational domain. The downside is the method requires a large amount of storage and solving a large system of equations. However, we succeed in reducing the storage requirement and computational time by splitting the matrix into the sum of a real symmetric matrix and a low-rank matrix. Consequently, we reduce computational time significantly by solving a smaller system having as many unknowns as the rank of the low-rank matrix. Furthermore, the splitting process allows us to separate the

temperature independent and dependent parts. We only compute the temperature independent part once. Therefore, we expect this would provide an advantage over FDTD method when electromagnetic fields are recomputed at each time step in the heat equation.

In effort to minimize the truncation error, we consider various approaches. First, we use the exact non-reflecting conditions for the propagating mode of the discrete equations at the truncated boundaries of the waveguide. This ensures no artificial reflection introduced to the computational domain by the numerical method. Second, we can use finer mesh size to achieve better accuracy. However, our method becomes inefficient as the mesh size getting smaller. For a finer grid with half the size of the previous discretization, the required storage increases by a factor of 16, and the method would take 64 times longer to solve the system by Gaussian elimination. In comparison, the FDTD method would only require 4 times the storage as before, and the computational time would increase by factor of 8 assuming the FDTD simulation reaches a harmonic steady state in a fixed period of time. Finally, we could increase accuracy by using the higher order stencil. This puts our method in a better light because there is virtually no increase in storage, and the system can still be splitted into the sum of a real symmetric matrix and a low-rank matrix as before.

We learn from the numerical results that the optimal length does not depend on the electrical conductivity σ as we expect. The optimal length for a lossless sample would be sufficient to optimize the energy deposition for a lossy sample. In addition, we find that the absorption power and the optimal length are highly dependent on the location of the sample. Theoretically, we should able to find the optimal location for a given sample using the system (3.15).

APPENDIX A

ASYMPTOTIC ANALYSIS IN A WAVEGUIDE

A.1 Asymptotic Analysis about a Symmetric Iris

This section reproduces the asymptotic analysis for a symmetric iris by Lewin [16] as shown in Figure (A.1). For the single mode TE waveguide, the modal representation
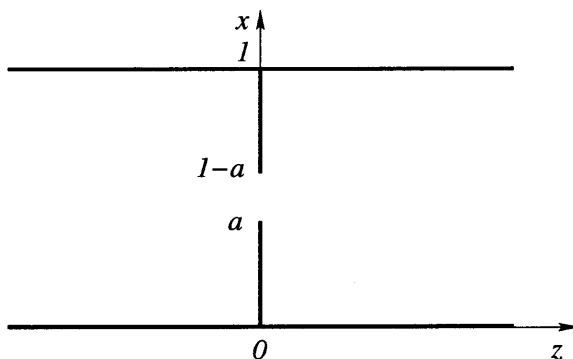
Figure A.1 A infinite waveguide with the presence of a symmetric iris.

of the solution inside an infinite waveguide with the presence of the iris located at $z = 0$,

$$
E_y = \begin{cases} \left(e^{ik_1 z} + Re^{-ik_1 z}\right) \sin\left(\pi x\right) + \displaystyle\sum_{m=2}^{\infty} R_m e^{k_m z} \sin\left(m\pi x\right), & z < 0, \\[2em] Te^{ik_1 z} \sin\left(\pi x\right) + \displaystyle\sum_{m=2}^{\infty} T_m e^{-k_m z} \sin\left(m\pi x\right), & z > 0, \end{cases}
$$

where $k_1 = \sqrt{k^2 - \pi^2}$ is the dimensionless wavenumber of the propagating mode, and $k_m = \sqrt{m^2\pi^2 - k^2}$ are the dimensionless wavenumbers of evanescent modes. At $z = 0$, $E_y = E\left(\pi x\right)$ in the aperture, and is zero elsewhere. Then, by the application of orthogonality and continuity of electric field in the aperture,

$$
1 + R = T = 2\int_a^{1-a} E\left(\pi x\right) \sin\left(\pi x\right) \, dx, \tag{A.1}
$$

$$
R_m = T_m = 2\int_a^{1-a} E\left(\pi x\right) \sin\left(m\pi x\right) \, dx. \tag{A.2}
$$

Similarly, continuity of the derivative of electric field with respected to z at $z = 0$ gives,

$$ik_1 (1 - R) \sin(\pi x) + \sum_{m=2}^{\infty} k_m R_m \sin(m\pi x)$$
$$= ik_1 T \sin(\pi x) - \sum_{m=2}^{\infty} k_m T_m \sin(m\pi x).$$

Rearranging terms,

$$ik_1 R \sin(\pi x) = \sum_{m=2}^{\infty} k_m R_m \sin(m\pi x).$$

Multiplying and dividing the left-handed side by T, then expressing T and R_m as in equations (A.1) and (A.2),

$$ik_1 \frac{R}{1 + R} \sin(\pi x) \int_a^{1-a} E(\pi\xi) \sin(\pi\xi)\, d\xi$$
$$= \sum_{m=2}^{\infty} k_m \sin(m\pi x) \int_a^{1-a} E(\pi\xi) \sin(m\pi\xi)\, d\xi.$$

Since $E(\pi x)$ vanishes at $x = a$ and $x = 1 - a$, we can employ the integration by parts. Let $\theta = \pi x$ and $\phi = \pi\xi$, then integration by parts yields,

$$\frac{ik_1}{\pi} \frac{R}{1 + R} \sin\theta \int_{\pi a}^{\pi(1-a)} E'(\phi) \cos\phi\, d\phi = \sum_{m=2}^{\infty} \frac{k_m}{m\pi} \sin(m\theta) \int_{\pi a}^{\pi(1-a)} E'(\phi) \cos(m\phi)\, d\phi.$$

Let $\delta_m = 1 - \dfrac{k_m}{m\pi}$, and $B = \dfrac{ik_1}{\pi} \dfrac{R}{1 + R}$.

$$B \sin\theta \int_{\pi a}^{\pi(1-a)} E'(\phi) \cos\phi\, d\phi = \sum_{m=2}^{\infty} (1 - \delta_m) \sin(m\theta) \int_{\pi a}^{\pi(1-a)} E'(\phi) \cos(m\phi)\, d\phi. \quad \text{(A.3)}$$

Evaluation of the integral equation (A.3) is relied on the fact that δ_m tends to zero as m increases. Hence, we can obtain the asymptotic approximation of B which in turn R and T by including appropriate δ_m terms. The method also replies on the orthogonality of cosine; therefore, we first bring the equation to proper form by

making the following change of variables.

$$\cos\theta = s\cos u, \text{ and } \cos\phi = s\cos v, \text{ where } s = \cos(\pi a). \tag{A.4}$$

The transformation (A.4) will give u and v a proper range $(0, \pi)$ as θ and ϕ vary from πa to $\pi(1-a)$. Next, we need to rewrite the summation in term of u and v. We notice that,

$$\sum_{m=1}^{\infty} \frac{\cos(m\theta)\cos(m\phi)}{m} = -\frac{1}{2}\log\left(2\left|\cos\theta - \cos\phi\right|\right) \tag{A.5}$$

With simple algebraic manipulation and the transformation (A.4), the right-handed side of equation (A.5),

$$\frac{1}{2}\log\left(2\left|\cos\theta - \cos\phi\right|\right) = \frac{1}{2}\log s + \frac{1}{2}\log\left(2\left|\cos u - \cos v\right|\right).$$

We can then rewrite the summation in term u and v.

$$\sum_{m=1}^{\infty} \frac{\cos(m\theta)\cos(m\phi)}{m} = -\frac{1}{2}\log s + \sum_{m=1}^{\infty} \frac{\cos(mu)\cos(mv)}{m}.$$

Differentiating equation (A.6) with respected to θ and rearranging the sum, we obtain the desired form,

$$\sum_{m=2}^{\infty} \sin(m\theta)\cos(m\phi) = -\sin\theta\cos\phi + \frac{\sin\theta}{s\sin u}\sum_{m=1}^{\infty} \sin(mu)\cos(mv).$$

Then, equation (A.3) becomes,

$$Bs^2\sin u \int_0^\pi E'(\phi)\frac{d\phi}{dv}\cos v\, dv$$

$$= \int_0^\pi E'(\phi)\frac{d\phi}{dv}\left[(1-s^2)\sin u\cos v + \sum_{m=2}^{\infty}\sin(mu)\cos(mv)\right] dv \tag{A.6}$$

$$- \frac{s\sin u}{\sin\theta}\int_0^\pi E'(\phi)\frac{d\phi}{dv}\sum_{m=2}^{\infty}\delta_m\sin(m\theta)\cos(m\phi)\, dv.$$

The first order of approximation is obtained by ignoring all δ_m terms, then equating the coefficients of $\sin(mu)$,

$$Bs^2 = 1 - s^2, \tag{A.7}$$

$$\int_0^\pi E'(\phi)\frac{d\phi}{dv}\cos(mv)\,dv = 0, \text{ for } m > 1. \tag{A.8}$$

Combining equations (A.4), (A.7) and the definition of B, we can solve for R.

$$R = \frac{-ib}{1+ib}, \text{ where } b = \frac{\pi}{k_1}\tan^2(\pi a).$$

From equation (A.8), we recognize that $E'(\phi)\dfrac{d\phi}{dv}$ is a multiple of $\cos v$ because of the orthogonality condition, i.e.

$$E'(\phi)\frac{d\phi}{dv} = B_1\cos v$$

With the trial function of this form, we can obtain higher order terms of the asymptotic series. Hence, the next term in the series involve δ_3, and the trial function is,

$$E'(\phi)\frac{d\phi}{dv} = B_1\cos v + B_3\cos(3v). \tag{A.9}$$

We note that the δ_{2n} terms vanish because of the symmetry of the problem. They correspond to the odd modes about the centerline $x = \dfrac{1}{2}$. Expressing other terms in equation (A.6) in term of u and v.

$$\cos(3\phi) = s^3\cos(3v) + 3s(s^2 - 1)cosv, \tag{A.10}$$

$$\frac{\sin(3\theta)}{\sin\theta} = \frac{s^2\sin(3u) + (s^2 - 1)\sin u}{\sin u}. \tag{A.11}$$

Substituting equations (A.9)–(A.11) into integrand equation (A.6), most of the terms in the series vanishes due to orthogonality. The contribution comes from two terms

$\sin u$ and $\sin(3u)$, and their coefficients satisfy the following linear system,

$$s(s^2 - 1)\delta_3 \left[s^3 B_3 + 3s(s^2 - 1)B_1\right] = B_1 \left[-s^2 B + 1 - s^2\right],$$

$$s^3 \delta_3 \left[s^3 B_3 + 3s(s^2 - 1)B_1\right] = B_3. \tag{A.12}$$

We can easily solve equation (A.12) to obtain R. The reflection coefficient R has the same form as before except b contains higher order term.

$$R = \frac{-ib}{1 + ib}, \quad \text{where } b = \frac{\pi}{k_1} \left[\tan^2(\pi a) - 3\delta_3 \frac{\sin^4(\pi a)}{1 - \delta_3 \cos^6(\pi a)}\right].$$

A.2 Asymptotic Analysis about a Lossy Target

This section derives the conservation of power inside an infinite waveguide in the presence of a lossy target. Recall that the electric field inside the waveguide and the
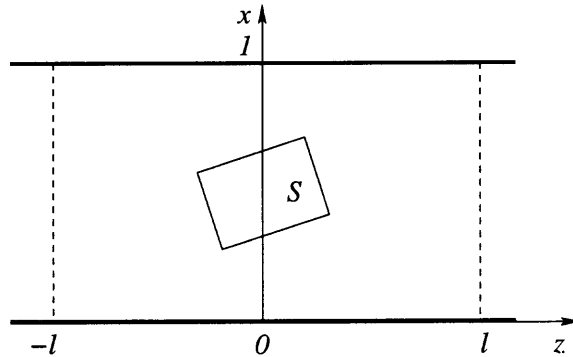
Figure A.2 A infinite waveguide with the presence of a lossy target.

target satisfies the Helmholtz equation (3.8),

$$\nabla^2 E_y + k^2[\epsilon + i\sigma(T)]E_y = 0. \tag{A.13}$$

Let u be the solution in which an incident wave of unit strength scattering the target from the left, the asymptotic solution far away from the target is

$$u = \begin{cases} \left(e^{ik_1 z} + R_\ell e^{-ik_1 z}\right) \sin(\pi x), & z \ll 0, \\ T_\ell e^{ik_1 z} \sin(\pi x), & z \gg 0. \end{cases} \tag{A.14}$$

Similarly, let v be the solution in which an incident wave of unit strength scattering the target from the right,

$$v = \begin{cases} T_r e^{-ik_1 z} \sin(\pi x), & z \ll 0, \\ \left(e^{-ik_1 z} + R_r e^{ik_1 z}\right) \sin(\pi x), & z \gg 0. \end{cases} \tag{A.15}$$

Since u and v satisfy the Helmholtz equation (A.13), their conjugates satisfy a similar equation, i.e.

$$\nabla^2 u^* + k^2[\epsilon - i\sigma(T)]u^* = 0. \tag{A.16}$$

Multiplying equation (A.13) by u^* with u replacing E_y as unknown quantity and equation (A.16) by u, then subtracting one equation from another, we have

$$u^*\nabla^2 u - u\nabla^2 u^* + 2ik^2\sigma(T)\,|u|^2 = 0. \tag{A.17}$$

Integrating equation (A.17) over the interior of the waveguide from $z = -l$ to $z = l$ as shown in Figure (A.2),

$$\int_V \left(u^*\nabla^2 u - u\nabla^2 u^*\right)\,dV + 2ik^2 \int_V \sigma(T)\,|u|^2\,dV = 0$$

Rewriting the first integrand as a divergent, and applying Gauss's divergence theorem which reduces the first volume integral to a surface integral.

$$\int_{\partial A} \left(u^*\frac{\partial u}{\partial n} - u\frac{\partial u^*}{\partial n}\right)\,dA + 2ik^2 \int_V \sigma(T)\,|u|^2\,dV = 0 \tag{A.18}$$

Since the electric field vanishes at the waveguide, the only contribution of the first integral comes from the ends ($z = \pm l$) of the waveguide. Furthermore, the electrical conductivity is zero outside the target, the second integral reduces to integral over the volume of the target. Thus, the equation (A.18) becomes,

$$\int_A \left(u^*\frac{\partial u}{\partial z} - u\frac{\partial u^*}{\partial z}\right)_{z=\pm l}\,dA + 2ik^2 \int_S \sigma(T)\,|u|^2\,dV = 0, \tag{A.19}$$

where A is the area of the waveguide and S is the volume of the target. For a sufficiently large l, we can evaluate the surface integral using the asymptotic solution (A.14), and obtain the conservation of power.

$$|R_\ell|^2 + |T_\ell|^2 = 1 - \frac{2}{A}\frac{k^2}{k_1}\int_S \sigma(T)\,|u|^2\,dV.$$

Similarly, we can obtain the same conservation of power in term of R_r and T_r using the asymptotic solution (A.15). We can derive another relation between R_ℓ, T_ℓ, R_r and T_r by replacing u^* with v^* in equation (A.17).

$$v^*\nabla^2 u - u\nabla^2 v^* + 2ik^2\sigma(T)uv^* = 0.$$

Following the same procedure as before, we obtain the same integral equation as (A.19) with v^* replacing u^*.

$$\int_A \left(v^*\frac{\partial u}{\partial z} - u\frac{\partial v^*}{\partial z}\right)_{z=\pm l} dA + 2ik^2\int_S \sigma(T)uv^*\,dV = 0,$$

Evaluating the surface integral at $z = \pm l$ using the asymptotic solutions (A.14) and (A.15), we arrive at another relation of R's and T's.

$$R_r^*T_\ell + R_\ell T_r^* = \frac{2}{A}\frac{k^2}{k_1}\int_S \sigma(T)uv^*\,dV.$$

For a symmetric and lossless target, $R_\ell = R_r$, $T_\ell = T_r$ and $\sigma = 0$, the relations reduces to,

$$\begin{aligned} |R|^2 + |T|^2 &= 1, \\ R^*T + RT^* &= 0. \end{aligned} \tag{A.20}$$

We also note the reflection and transmission coefficients of the iris in §A.1,

$$R = \frac{-ib}{1+ib}, \text{ and } T = 1 + R,$$

automatically satisfy the relations (A.20) for any b not equal to i.

APPENDIX B

ENERGY FLOW IN A WAVEGUIDE

In order to initiate the numerical process, we need to know the amplitude E_0 of the electric field which is usually given in term of input power P. And, power relates to electromagnetic fields through the Poynting vector [17].

$$\mathbf{S} = \frac{1}{2}\left(\mathbf{E} \times \mathbf{H}^*\right) = \frac{1}{2}\left(E_y H_z^* \hat{\mathbf{x}} - E_y H_x^* \hat{\mathbf{z}}\right),$$

for a TE mode. Then, the total power flow is given by the integral of the axial component of $\mathbf{S}$ over the cross-sectional area of the waveguide.

$$P = \int_A \mathbf{S} \cdot \hat{\mathbf{z}}\, da = -\frac{1}{2}\int_A E_y H_x^*\, da$$

Since $\mathbf{H} = -\dfrac{i}{\mu_0 \omega}\nabla \times \mathbf{E}$, then $H_x = \dfrac{i}{\mu_0\omega}\dfrac{\partial E_y}{\partial z}$. Thus, the total power P becomes,

$$P = \frac{i}{2\mu_0\omega}\int_A E_y \frac{\partial E_y^*}{\partial z}\, da. \tag{B.1}$$

In a single-mode rectangular waveguide,

$$E_y = E_0 e^{ik_1 z/W}\sin\left(\frac{\pi x}{W}\right).$$

Substituting above expression into equation (B.1), we obtain,

$$P = \frac{k_1 E_0^2}{2\mu_0\omega W}\int_A \sin^2\left(\frac{\pi x}{W}\right)\, da = \frac{k_1}{\mu_0\omega W}\frac{A E_0^2}{4}.$$

Simplifying above express by substituting $k = \dfrac{\omega W}{c}$ and $Z_0 = \sqrt{\dfrac{\mu_0}{\epsilon_0}}$.

$$P = \frac{k_1 A E_0^2}{4k Z_0}.$$

Hence,

$$E_0 = 2\sqrt{\frac{kZ_0P}{k_1A}}.$$

For a waveguide with the height is half of its width,

$$E_0 = \sqrt{\frac{8kZ_0P}{k_1W^2}}.$$

REFERENCES

[1] C. V. Hile and G. A. Kriegsmann, "A hybrid numerical method for loaded highly resonant single mode cavities," *J. Comput. Phys.*, vol. 142, no. 2, pp. 506–520, 1998.

[2] M. Iskander, R. Smith, A. Andrade, J. Kimrey, H., and L. Wal, "FDTD simulation of microwave sintering of ceramics in multimode cavities," *IEEE Trans. Microwave Theory Tech.*, vol. 42, no. 5, pp. 793–800, 1994.

[3] Z. Huang, J. Tucker, and M. Iskander, "FDTD modeling of realistic microwave sintering experiments," in *Antennas and Propagation Society International Symposium, 1994. AP-S. Digest*, vol. 3, (Seattle, WA), pp. 1798–1801, Jun. 1994.

[4] M. Subirats, M. Iskander, and M. J. White, "FDTD simulation of microwave sintering in large (500/4000 liter) multimode cavities," in *Microwave Processing Mater. V, Mater. Res. Soc. Symp. Proc.*, vol. 430, (San Francisco, CA), pp. 29–36, Apr. 1996.

[5] D. D. Dincov and K. A. Parrott, "Computational analysis of microwave heating patterns in resonant multimode cavities," in *Proceedings of the 2004 ACM symposium on Applied computing*, (New York), pp. 215–219, ACM Press, 2004.

[6] A. Bayliss, C. I. Goldstein, and E. Turkel, "The numerical solution of the Helmholtz equation for wave propagation problems in underwater acoustics," *Comput. Math. Appl.*, vol. 11, no. 7-8, pp. 655–665, 1985. Computational ocean acoustics (New Haven, Conn., 1984).

[7] H. Yserentant, "On the multilevel splitting of finite element spaces for indefinite elliptic boundary value problems," *SIAM J. Numer. Anal.*, vol. 23, no. 3, pp. 581–595, 1986.

[8] H. C. Elman, O. G. Ernst, and D. P. O'Leary, "A multigrid method enhanced by Krylov subspace iteration for discrete Helmhotz equations," *SIAM J. Sci. Comput.*, vol. 23, no. 4, pp. 1291–1315 (electronic), 2001.

[9] L. Abrahamsson and H.-O. Kreiss, "Numerical solution of the coupled mode equations in duct acoustics," *J. Comput. Phys.*, vol. 111, no. 1, pp. 1–14, 1994.

[10] D. R. Croft and D. G. Lilley, *Heat Transfer Calculations Using Finite Difference Equations*. London: Applied Science, 1977.

[11] G. H. Golub and C. F. Van Loan, *Matrix Computations*. Baltimore, London: The Johns Hopkins University Press, 3rd ed., 1996.

[12] M. Frigo and S. G. Johnson, "Fastest Fourier Transform in the West," *2003*, <http://www.fftw.org>, (visited 26 Jun. 2004).

[13] L. C. Thomas, *Heat Transfer*. New York: McGraw-Hill, 1953.

[14] R. E. Bolz and G. L. Tuve, *CRC Handbook of Tables for Applied Engineering Science*. Cleveland, Ohio: CRC Press, 2nd ed., 1973.

[15] W. R. Veazey and C. D. Hodgman, *CRC Handbook of Chemistry and Physics*. Cleveland, Ohio: Chemical Rubber Pub. Co., 57th ed., 1976.

[16] L. Lewin, *Theory of Waveguides*. New York: Wiley, 1975.

[17] J. D. Jackson, *Classical Electrodynamics*. New York: Wiley, 3rd ed., 1999.